

A CASE FOR $H_0 = 42$ AND $\Omega_0 = 1$ USING LUMINOUS SPIRAL GALAXIES AND THE COSMOLOGICAL TIME SCALE TEST

ALLAN SANDAGE

Center for Astrophysical Sciences in the Department of Physics and Astronomy, The Johns Hopkins University; and
 Space Telescope Science Institute

Received 1987 May 29; accepted 1987 September 9

ABSTRACT

There are two internally self-consistent methods of finding the Hubble velocity-distance ratios for individual galaxies. In the first, one assumes a linear velocity-distance relation, from which *relative* distances are found from the velocities. A system of absolute magnitudes is obtained thereby, later zero-pointed using Cepheid distances to local calibrating galaxies. In the second, one uses some parameter such as 21 cm line width, or the internal velocity dispersion, or the de Vaucouleurs Λ -index, etc., to which is assigned a *fixed* absolute magnitude $\langle M \rangle$ for each value of the parameter, again zero-pointed later from the Cepheid calibrating galaxies.

Neither of the two methods can be faulted by considering only the internal data of a flux-limited sample, yet one or the other gives the wrong mean Hubble constant unless external information is known, either on the form of the velocity field (i.e., whether the redshift-distance relation is linear), or on the dispersion of the luminosity function. The self-consistency can be broken by adding data from a fainter flux-limited sample, seeking a contradiction in one of the methods.

The test of which method is in error, and therefore whether the high or low value of H_0 is correct, is made here by combining redshift and magnitude data for bright ScI galaxies from the RSA with faint ScI galaxies from two catalogs in the literature to demonstrate the bias in the second method directly. It is shown that the method of assigning a fixed $\langle M \rangle$ to each ScI galaxy in the bright sample (or to any other parameter that might be adopted as a distance indicator) produces an artificially compressed distance scale, imitating a varying Hubble ratio that appears to increase outward. However, adding the bright and faint samples gives a list that approaches a volume-limited catalog for redshifts smaller than $\sim 4000 \text{ km s}^{-1}$, from which it is demonstrated that (1) the local velocity-distance relation is linear over this redshift range (2), the ScI luminosity function is broad with $\sigma \langle M \rangle = 0.7 \text{ mag}$, and (3) the value of the Hubble constant is low.

Calibration of the ScI magnitude and redshift data in the $v \rightarrow 0$ limit, using M31, M81, and M101 as calibrators, gives

$$H_0 = 42 \pm 11 \text{ km s}^{-1} \text{ Mpc}^{-1},$$

where the error is estimated by assigning an absolute magnitude uncertainty of 0.6 mag for the combined errors of (1) the calibration of the relevant ScI zero point from only three local galaxies, and (2) the uncertainty of the apex magnitude ($\langle M_{B_T} \rangle$ at $v \rightarrow 0$) which is determined from the upper and lower envelope fits to the $M_{B_T}, \log v_0$ diagram. Cepheid distances to many more ScI calibrating galaxies, and a complete (volume-limited) survey for such galaxies will be needed to improve the value of H_0 via this method.

The age of the globular clusters is adopted to be $13.5 \pm 1 \text{ Gyr}$ from the precision measurement of the age of 47 Tuc (Hesser *et al.*) using Vandenberg isochrones that permit $[\text{O}/\text{Fe}]$ to vary with $[\text{Fe}/\text{H}]$, now required from the recent subdwarf data. From the globular cluster age, plus the gestation period of galaxies, the age of the universe is put at $14.9 \pm 2 \text{ Gyr}$, giving $H_0 T_U = 0.64 \pm 0.19$ and thereby

$$\Omega_0 = 1.2^{+3.9}_{-0.9}.$$

Although the errors on Ω_0 are large, the increase in the H_0^{-1} Hubble time to $\sim 23 \text{ Gyr}$ if $H_0 = 42$, and the decrease in the globular cluster ages to $\sim 14 \text{ Gyr}$ now permits $\Omega_0 = 1$ with $\Lambda = 0$ from the time scale test, whereas earlier literature values on ages did not.

Subject headings: cosmology — galaxies: distances

I. INTRODUCTION

After ~ 50 years of effort—some sporadic, some intense—the Gauss-Riemann space-time scalar curvature (kc/R) is not yet accurately known. Hubble (1936c) attempted to measure it directly from galaxy counts, following the method of experimental geometry begun by Gauss and by Schwarzschild. He used a semi-heuristic method (Hubble and Tolman 1935) to relate apparent magnitudes and redshifts to distances in a

program aimed at finding a deviation of the measured volume from that expected in Euclidean space.

Hubble's 1936 conclusion concerning the value of R^{-1} was inconclusive for a variety of reasons. Some were technical concerning magnitude scale errors (Stebbins, Whitford, and Johnson 1950), an inadequate definition of total galaxy magnitudes (Humason, Mayall, and Sandage 1956, hereafter HMS, appendix A), imprecise knowledge of the K -effect of redshifts

on magnitudes (Greenstein 1938; HMS 1956, Appendix B; Oke and Sandage 1968; Lasker 1970; Whitford 1971), etc. Some were conceptual such as the use of inappropriate definitions of the proper distance–magnitude–redshift relations for different geometries (Hubble and Tolman 1935 compared with Mattig 1958, 1959; Sandage 1961*a*, 1962) because the precise theory was unknown until Mattig derived the equations in closed form.

The geometry of space-time is measured either by the deceleration parameter q_0 [related to R_0^{-1} by $k^{1/2}cR_0^{-1} = H_0(2q_0 - 1)^{1/2}$] or by the ratio, Ω_0 , of the present-day density to the closure density $3H_0^2/8\pi G$. The relation between them is $\Omega_0 = 2q_0 + 2/3\Lambda c^2/H_0^2$ if we wish to retain a nonzero cosmological constant, Λ . From the requirement of grand unification for inflation in the early universe so as to achieve both the present-day near-flatness and the observed homogeneity of the Gamow-Alpher-Herman 3 K radiation, Ω_0 must be infinitesimally close to 1 except in highly contrived circumstances. The primary aim of observational cosmology is then to measure an accurate value of either q_0 from geometry, or Ω_0 from dynamics to test these predictions of the connection between classical cosmology and particle physics, brought about by the grand unification hypothesis.

There are four known direct ways to q_0 , but only the time-scale test is robust. (1) The $N(m)$ count test is degenerate in q_0 to first order in z (Sandage 1961*a*; Robertson and Noonan 1968; Misner, Thorne, and Wheeler 1973), and is highly sensitive to luminosity evolution in the look-back time (Brown and Tinsley 1974). The $N(z)$ test recently applied by Loh and Spillar (1986) requires precise knowledge of the incompleteness of the counts in any redshift bin $z^2\Delta z$. This knowledge is almost impossible to obtain, given the available sampling procedures using galaxies with their large range of surface brightness and absolute luminosities. (2) Luminosity evolution is the stumbling block for the best known of the tests via the $m(z)$ Hubble diagram. (3) Evolution of linear sizes with time or with the absolute radio power also complicates the angular diameter–redshift, $\theta(z)$, test (cf. Miley 1971; Kapahi 1975, 1987; Swarup 1975; Hickson 1977; Bruzual and Spinrad 1978). The problem common to these three classical tests is the variation with time of some measured property of the galaxies that mark the space. On the other hand, the time-scale test is *evolution-free* because we only compare two time scales, each of which is independent of secular variations of the measured parameters.

The time since the beginning of the expansion, T_E , depends only on the density parameter Ω_0 and the Hubble time constant, H_0^{-1} for those Friedman models with $\Lambda = 0$ (Sandage 1961*a*, § V). For models where $\Lambda \neq 0$, the calculations by Refsdal, Stabell, and de Lange (1967), following Solheim (1966), are complete over the relevant parameter range of T_E , Ω_0 , Λ , and H_0^{-1} . The test is made by comparing $T_E = f(\Omega_0, \Lambda)H_0^{-1}$ with the age of the universe, T_U , determined from some independent age dating method. The numerical value of f constrains the acceptable range of Ω_0 and Λ (Robertson 1955, Fig. 3; Sandage and Tammann 1984, Figs. 6 and 9; 1986 Figs. 6 and 8). If $f = \frac{2}{3}$ and $\Lambda = 0$, then $\Omega_0 = 1$ exactly. Even if not, Ω_0 can be determined by the comparison of T_E and T_U .

Clearly, the present dichotomous value of H_0 near either 50 or 100 km s⁻¹ Mpc⁻¹ is intolerable for the test. No satisfactory critical analysis has yet appeared in the literature contrasting the two methods of using redshifts combined with some distance-indicating parameter (e.g., angular size, apparent magnitude, Hubble type, 21 cm line width, etc.) to find H_0 . The two general methods of using the data differ only in

whether the *redshift* or the *other parameter* (magnitude, 21 cm line width, etc.) is used as independent variable. The purpose of this and the following paper is to show that this seemingly trivial choice is the cause of the present disagreement over H_0 rather than any difference in the input data for the local calibrators. A review of the general agreement for the very local distance scale to the calibrating galaxies and the problem of the bias is given by Tammann (1987).

In this first paper we compare the two principal methods of treating the data and show therein that one route to H_0 is flawed by selection effects when using flux-limited catalogs. The proof is made by analyzing two sets of catalogs that reach different apparent flux levels. In this way, the selection effects are shown directly. In the following sections we analyze the optical data on field spiral galaxies of the brightest van den Bergh luminosity class. Calibration using M31, M81, and M101 which have Cepheid distances gives $H_0 = 42 \pm 11$ km s⁻¹ Mpc⁻¹. A similar analysis and a similar result that H_0 is low (~ 55 km s⁻¹ Mpc⁻¹) is given in the following paper using 21 cm radio line width data. The exact value that we derive is not the purpose of this paper. Rather, it is to show that all values of H_0 derived by the method of assigning an $\langle M \rangle$ value to any given distance indicator is subject to systematic error, giving too large an H_0 value if uncorrected for bias.

As to the *form* of the expansion, the empirical proof given here that the apparent increase of H_0 with distance (Hawkins 1962; de Vaucouleurs 1972; Segal 1975, 1981, 1982; Nicoll and Segal 1982 in answer to Soneira 1979; de Vaucouleurs and Peters 1986; Giraud 1985, 1986*a, b*) is a result of selection bias is an extension of a previous argument (Sandage, Tammann, and Yahil 1979, hereafter STY) that used only field galaxies brighter than apparent magnitude ~ 13 , and is parallel to the formal proof via the Malmquist bias equations given by Teerikorpi (1975*a, b*; 1984) and applied by Bottinelli *et al.* (1986). The conclusions of the three sets of studies agree that the very local Hubble velocity field *is* linear and that the value of H_0 is low.

II. TWO SECONDARY METHODS TO DETERMINE DISTANCE RATIOS

We suppose in what follows that data on redshift and apparent magnitude (or any other supposed distance indicator such as angular diameter, or Hubble type, or luminosity class) exist for galaxies in a catalog such as the RSA (Sandage and Tammann 1981) that is complete in redshift and complete also to a given flux limit, or whose incompleteness function is known (cf. Tammann, Yahil, and Sandage 1979, hereafter TYS).

After the primary distance indicators such as Cepheids or bright resolved stars have been exhausted because of insufficient range, only methods using secondary brighter indicators are available. Two different methods are being used in the current literature to obtain distances far beyond the Local Group. Because these two distance scales progressively diverge with increasing distance, at least one of them must be wrong. The methods are as follows.

1. In the first it is assumed that an ideal *linear* redshift–distance relation exists, justified by the data on nearby clusters, groups, and local galaxies with Cepheid distances (Sandage 1972*a, b, c*, 1975, 1986; Sandage and Tammann 1975*a*, 1985; Sandage, Tammann, and Hardy 1972). From the ratios of the redshifts we can then obtain relative distances. Further, if we adopt a working value of H_0 (later to be determined), the absolute magnitude M_i can be calculated for any galaxy i from

its apparent magnitude m_i and from the distance given by $r_i = v_i/H_0$. The zero point of the absolute magnitude scale is then calibrated using Cepheid distances to suitable local galaxies.

2. In the second method it is assumed that any indicator such as the van den Bergh luminosity index for a given galaxy type, or a given 21 cm line width, has a stable mean value $\langle M \rangle$. One then applies $\langle M \rangle$ to each galaxy i , from which individual distance moduli $m_i - \langle M \rangle$ are obtained, and thereby individual Hubble ratios $h_i = v_i/r_i$ using $r_i = \text{dex} [0.2(m - M + 5)]$.

For each method one proceeds to the mean Hubble constant for the sample as follows. In method (1) the mean M_i values are compared with $\langle M_i \rangle$ from the local calibrating galaxies that have Cepheid distances such as M31, M81, and M101 for luminosity class I systems. To find the proper value of $\langle M_i \rangle$, the data for the field sample must be read at the redshift limit of $v_i \rightarrow 0$ which defines the volume element of the local calibrators. The working value of H_0 is then changed by requiring that this mean $\langle M_i \rangle$ for the field sample be the same as for the local calibrators (§ VI) in the redshift limit of $v_i \rightarrow 0$. In method (2) we use the individual $h_i = v_i/r_i$ values, which then must be corrected for the bias caused by the flux-limited nature of the data before a correct $\langle H_0 \rangle$ value is found.

The two methods address different questions. In the first we adopt a linear velocity–distance relation and find properties of $\langle M \rangle$ thereby. In the second we adopt a fixed $\langle M \rangle$ for every galaxy in the subset and from the resulting parameter distance r_i one attempts to find properties of the Hubble flow itself as if v_i , rather than r_i , is suspect. Note again that the difference between the methods is in which parameter (v_i or $\langle M \rangle$) coupled with m_i is taken to be the independent variable.

If the local velocity field is indeed linear, we demonstrate later (Fig. 9) that the results of each method converge to the same value of H_0 , as the flux limit of the sample is progressively decreased to form a data subset that approaches a distance-limited sample. However, the methods do not give the same result when a given flux-limited catalog is analyzed by either (a) using an incorrectly narrow luminosity function $\Phi(M)$ in method (2), or (b) by ignoring the bias, which is equivalent to assuming an infinitely narrow delta function for $\Phi(M)$. Because the luminosity function is not known *a priori*, there is no *a priori* way to decide between the methods except by comparing a faint and a bright catalog.

Because each method is self-consistent in the absence of external data on $\Phi(M)$, a decision between them can only be made either from (1) an independent knowledge of the true luminosity function (the method of TYS 1979, by adopting the great cluster function) or (2) by sampling fainter apparent magnitudes in a general field catalog to approach a distance-limited sample for at least part of the data set—our present route.

a) Expected Distribution of M_i in a Flux Limited Sample Using a Linear Velocity-Distance Relation

The steps to be followed in method (1) are the following.

a. Assume $r_i = v_i/H_0^A$ where H_0^A is an arbitrarily adopted number to be adjusted later (§ VI) via the local calibrators.

b. For every galaxy in the sample, calculate the kinematic distance r_i from v_i/H_0^A and then calculate M_i from $M_i = m_i + 5 - 5 \log r_i$.

c. Construct a “bias diagram” by plotting M_i versus $\log v_i$ (or $m_i - M$) for the total sample. This diagram is useful to test if bias is present. Examples are Figure 7 of Sandage (1972c) where the increase of radio power as z^2 for 3CR radio sources

is clearly due to selection bias, and Figures 1 and 3 of STY where the bias of the RSA sample is shown.

A demonstration of the usefulness of the M_i , $\log v$ diagram is the Monte Carlo simulation by Spaenhauer (1978). A different version of his original diagram is shown as Figure 1 here, also calculated by Spaenhauer for Tammann’s (1987) review given elsewhere. The top panel shows the distribution of M_i for a complete distance-limited sample whose luminosity function is Gaussian with a dispersion of $\sigma = 2.0$ mag. Because the volume enclosing the sample increases with increasing distance, the bright and faint envelope lines open out. These envelopes define the M_i values where the luminosity function $\Phi(M) = 1$ in both its bright and faint wings.¹

If we were to assign the mean absolute magnitude $\langle M \rangle$ that is appropriate for the complete distribution to every galaxy in a distance-limited sample, we would make as many mistakes toward the bright end as the faint, and the mean $\langle \log r_i \rangle$ for the complete sample would not be a function of distance. However, in flux-limited data sets the sample is truncated by the flux limit of the catalogs, with the consequence that different fractions of $\Phi(M)$ are sampled at different distances (Fig. 1b). This produces an artificial increase in absolute luminosity with distance which is the Malmquist bias.

Note that if method (2) is used to analyze such a truncated sample, where a fixed $\langle M \rangle$ is applied to all galaxies without regard for the bias, then progressively incorrect values of $\langle \log r_i \rangle$ will be obtained as the distance is increased. To test if this is the origin of the divergence of the distance scales in the current literature all we need to do is to change the limit line in Figure 1 toward fainter apparent magnitudes. For if the apparent increase in $\langle M \rangle$ with distance in Figure 1b is due to bias, i.e. is not caused by incorrectly using a linear velocity–distance relation if it is really nonlinear, then the fainter galaxies analyzed using method (1) will begin to fill the region between $m = 13$ and a fainter line at $m = 15.5$, say. However, if the velocity–distance relation is not linear, then the apparently fainter galaxies will continue the apparent trend of $\langle M_i \rangle$, either seeming to become even brighter with increasing distance or will tack on in a continuous manner to the end of the trend in Figures 1b or 4b.

b) Expected Distribution of the Apparent Hubble Ratio Using Method (2) without Bias Correction

The steps to be followed in method (2), making no *a priori* assumption on the form of the velocity–distance relation, are:

a) assign a fixed value of $\langle M \rangle$ to each galaxy i ;

b) form $m_i - \langle M \rangle$ for each galaxy and calculate the photometric distance r_i from $m_i - \langle M \rangle + 5 = 5 \log r_i$;

c) use the observed velocity (corrected to the Local Group centroid and for Virgocentric infall if desired) to obtain the Hubble ratio $h_i = v_i/r_i$ for each galaxy;

d) plot h_i versus $\log v_i$ (or $\log r_i$) to determine the nature of the local velocity field.

We note again that it is impossible to decide between the

¹ The σ value of 2 mag in Figure 1 is larger than the $\sigma = 0.7$ mag appropriate for ScI galaxies. This, however, is of no consequence in illustrating the principle of the bias problem in flux-limited samples. The same type of variation $\langle M \rangle$ with distance that is shown in Figure 1 is present in every such sample whenever $\sigma(M) \neq 0$. The amplitude of the $\langle M \rangle = f(D)$ variation, of course, depends on the $\sigma(M)$ value. The point is that diagrams isomorphic to Figure 1 are obtained by changing σ to any desired value, together with a corresponding change in the scale of the ordinate. Figure 11 later here shows such a set of isomorphic diagrams for different values of $\sigma(M)$.

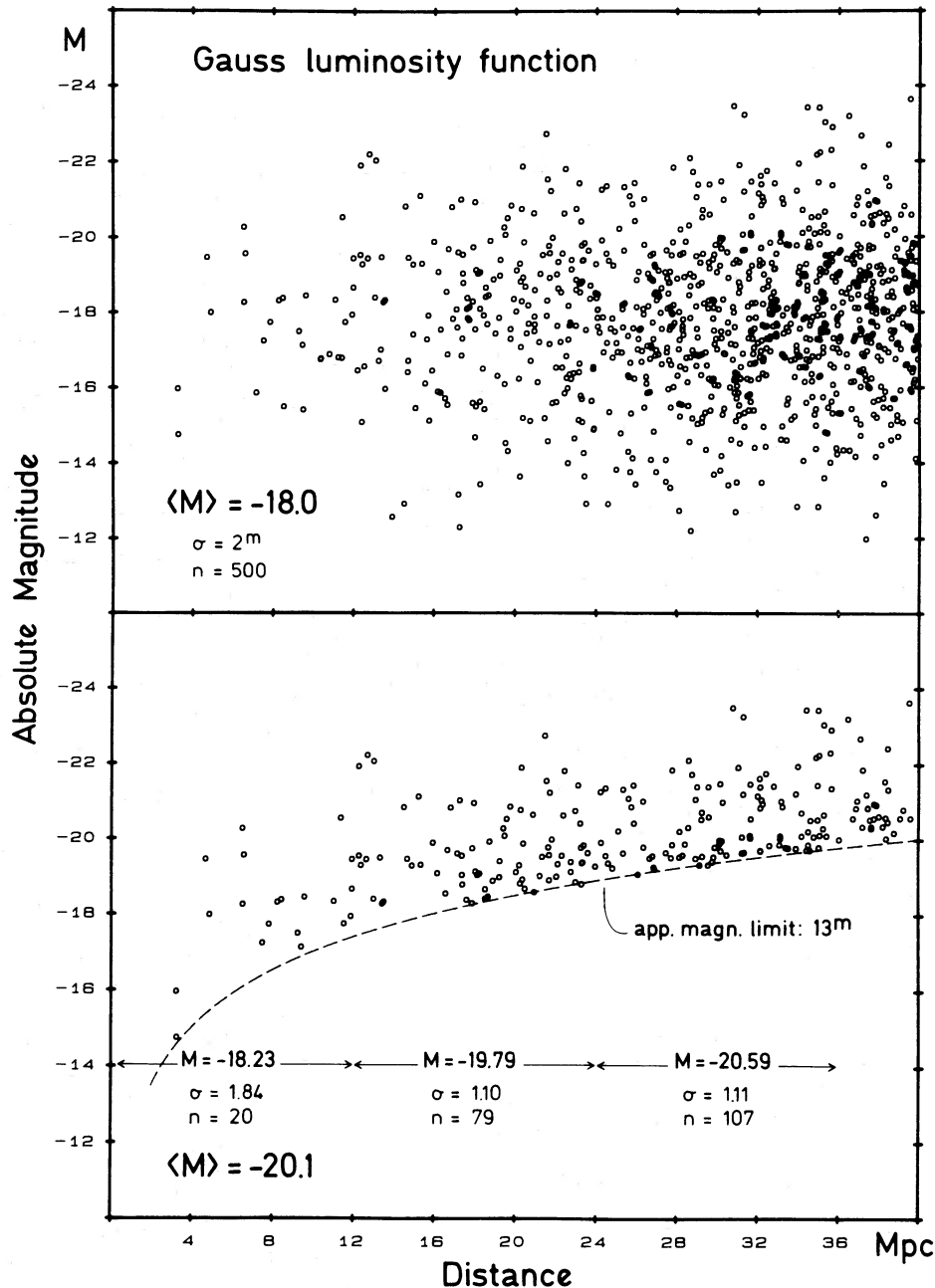


FIG. 1.—Monte Carlo simulation by Spaenhauer of the distribution of absolute luminosities if $\Phi(M)$ is a Gaussian with $\sigma = 2.0$ mag and $H_0 = 50$ km s $^{-1}$ Mpc $^{-1}$. *Top*: Distribution of M for a complete sample of galaxies in a given volume. The upper and lower envelope lines open symmetrically about the assumed mean absolute magnitude $\langle M \rangle$. *Bottom*: The distribution that would be observed in a flux-limited sample, cut at $m = 13$ mag. The observed $\langle M \rangle$ becomes brighter with increased distance due to the imposed flux-limit on the complete sample. If the abscissa had been given as log distance, the lower flux limit-line would have been straight.

results of method (1) and (2) if the luminosity function is unknown and if only a single data sample to a given flux limit is available. This is why adding a fainter data set to the RSA sample is so important in deciding if there is a nonlinear velocity field in which H_0 increases outward, or whether $\Phi(M)$ is broad and the very local velocity field is *linear*, meaning that H_0 is constant with distance.

III. REDSHIFT AND MAGNITUDE DATA FOR LUMINOUS SPIRALS FROM SAMPLES WITH DIFFERENT FLUX LIMITS

Galaxies of a particular Hubble type can be used as relative distance indicators if they have a moderately narrow range of

intrinsic luminosities. Hubble (1936*a, b*) was the first to suggest that a near Gaussian $\Phi(M)$ distribution exists for galaxies of high surface brightness—i.e., those which had redshift and magnitude data in the mid-1930s. He obtained $\sigma(M) = 0.84$ mag for his particular sample that contained both spirals and E systems.

Due to the statistical problems with flux-limited samples in this and in subsequent studies of the same kind (cf. HMS 1956), the conclusion of a narrow $\Phi(M)$, even one *bounded* at the faint end, was questioned (Zwicky 1957). However, van den Bergh (1960*a, b*) demonstrated that late-type galaxies could be divided into luminosity classes on the basis of appearance, that

$\langle M \rangle$ in the flux-limited sample defined by the HMS catalog changed progressively with his classes, and because no faint ScI galaxies were seen in the Shapley-Ames list, that $\Phi(M)$ for spirals did not increase exponentially at faint luminosities.

The next step was the demonstration that ScI galaxies in a fainter sample than the RSA continued to define a restricted band in the $m, \log v$ Hubble diagram (Sandage and Tammann 1975*b*, Fig. 1) rather than to merely increase the apparent magnitude scatter at a given redshift, which would have indicated a very broad $\phi(M)$. The magnitude residuals at a given velocity for the RSA sample, combined with the fainter sample, continued to have nearly a Gaussian distribution with $\sigma(M) = 0.6$ mag.

However, the idea of a moderately narrow $\Phi(M)$ for spirals (especially for luminosity classes $> \text{II}$) was then questioned by TYS (1979) in their analysis of the RSA data to obtain the correction due to the flux-limited sample. The idea was defended by Kennicutt (1982), and his result was discussed by Kraan-Korteweg, Sandage, and Tammann (1984, KKST) who showed that the local velocity perturbation had negligible effect on the calculated $\phi(M)$. It was then demonstrated from the distance-limited sample in the Virgo Cluster (Binggelli, Sandage, and Tammann 1985; Sandage, Binggelli, and Tammann 1985*b*, hereafter SBT, Figs. 4, 7, and 18) that Kennicutt's conclusion is, indeed, correct that a usefully narrow $\Phi(M)$ does exist² for spirals.³

a) Data from the RSA

It was known from HMS (1956) that apparent magnitudes are well correlated with redshifts for bright field galaxies. However, the HMS data sets for each Hubble type show a shallower slope in the m, v correlation than $m \sim 5 \log v$ (HMS 1956, Figs. 3–12; Hawkins 1962). In this section we show that the same is true for the Sb and Sc galaxies of luminosity class I and I–II in the RSA. The result is similar to that discussed for E and SO galaxies by STY (1979), which was shown there to be explained by the Malmquist bias if the field $\Phi(M)$ is closely the same as for the great clusters. It needs to be emphasized that we require no such assumption on $\Phi(M)$ in the demonstration made here in which we add a fainter sample.

Data for Sb, Sbc, and Sc galaxies of luminosity classes I–I.3 and I–II are listed in Table 1, taken from the second edition of the RSA (Sandage and Tammann 1987). Column (3) shows the adopted velocity, reduced to the centroid of the Local Group

² The discussion by KKST centered on whether the inclusion of a Virgo velocity perturbation in the calculations did, in fact, make $\phi(M)$ narrower than without the correction. The seeming difference between the TYS and the Kennicutt conclusions was due to different representation of $\phi(M)$ appearing to differ in their narrowness. TYS viewed $\phi(M)$ in its log form; Kennicutt plotted the data more directly as $\phi(M)$ itself, whose visual impression is for a much narrower distribution.

³ The de Vaucouleurs Λ index is a generalization of the variation of $\langle M \rangle$ along the Hubble sequence and among the van den Bergh luminosity classes, correcting for the variation of the gross Λ - M correlation which exists, albeit with a dispersion whose size is still under discussion (SBT 1985*a*; de Vaucouleurs and Corwin 1986*a*). Note that if a sample is restricted to say ScI galaxies alone, the discussion is, then, necessarily restricted to a particular de Vaucouleurs Λ -value. Therefore, the demonstration made here of selection effects for ScI galaxies can be generalized to apply to other discussions of the distance scale that use say Λ for galaxies along some range of the Hubble sequence, or 21 cm line width (Aaranson *et al.*, 1982; Giraud 1985, 1986*a, b*), or corrected internal velocity dispersion σ_D (Dressler *et al.* 1987), or H β flux of H II regions (Melnick, Terevich, and Moles 1987), etc., each of which uses method (2), and hence all are suspect.

as listed in column (20) of the RSA. Column (4) is the velocity correction for Virgocentric infall calculated by Kraan-Korteweg (1986) using $v = 220 \text{ km s}^{-1}$ for the Local Group infall in the density model she adopts. Column (5) is the log of columns (3) plus (4). The "total" blue magnitude B_T from column (12) of the RSA is in column (6). The magnitude in column (7) is corrected for galactic and internal absorption taken from column (15) of the RSA. Absolute magnitudes, calculated as if $H_0 = 50 \text{ km s}^{-1} \text{ Mpc}^{-1}$, are listed in columns (8), (9), and (10) with and without internal absorption corrections, and using the velocities in column (3) for the listings in (8) and (9) or in column (5) for the listing in column (10).

The v_0^{220} , B_T^{220} , and Sc galaxies of luminosity classes I–I.3 and I–II is shown in Figure 2. Small magnitude corrections have been applied to the Sbc and Sb galaxies to reduce them to the same mean luminosity as for the ScI–I.3. These corrections, shown in the code to the diagram, were determined by plotting the v, B_T diagrams for each type separately from the data in Table 1, and finding the offset in the distribution of points relative to the ScI data simply by sliding one diagram over any other.

The envelope and ridge lines in Figure 2, drawn to guide the eye, have a slope of 5, required if the local velocity field is linear and if there are no selection effects in the data. The data clearly deviate from this slope, showing brighter magnitudes at higher velocities relative to the ridge line. This is the same sense as in HMS (Figs. 3–10) and in the E and SO galaxies of the RSA (STY 1979).

In Figure 3 we show data with and without correction for internal absorption (CIA) and using v_0 velocities uncorrected for Virgo infall. The purpose is to illustrate that these corrections are minor and do not alter the situation. A least-squares line through the data in both Figures (2) and (3) and later in Figure (6) has a smaller slope than 5.

b) The $M_{B_T}, \log v_0$ Bias Diagram

The consequence of this slope difference from 5 in Figures 2 and 3 is that the M_{B_T} which is calculated using $r_i = v_i/H_0$ varies progressively with $\log v_0$ for galaxies in the sample, shown in Figure 4*a*. The variation is clear and, as previously discussed, is either what is expected due to bias in a flux-limited sample (Fig. 1*b*), or is due to a real departure of the local velocity field from the assumed linearity.

For later reference we show upper and lower envelope lines in Figure 4*b* that enclose the distribution. Also shown is the apparent magnitude limit of the RSA, put at $m_{0,i} = 12.5$ which is the approximate catalog limit corrected for an internal absorption of ~ 0.4 mag for Sc galaxies.

The arrow in Figure 4*b* put at $M_{B_T}^i(H_0 = 50) = -21.0$ is the apex where the two envelope lines, assumed to be symmetrical due to an assumed symmetrical $\Phi(M)$, meet in the $v \rightarrow 0$ limit. This is an important point in the final determination of H_0 using the local calibrators (§ VI).

c) Data from the Fainter ScI Samples

To decide between the two explanations of Figure 4*a* (i.e., bias or nonlinear velocity field) we now add fainter ScI galaxies. Two samples of such galaxies exist. A catalog of 69 ScI galaxies between $m = 13$ and ~ 15.7 , chosen by inspecting the POSS original plates, with redshifts measured at Palomar, was made by Sandage and Tammann (1975*b*), hereafter called the S-T sample. An independent catalog of 202 such galaxies was made by Rubin *et al.* (1976) in their search for large-scale devi-

TABLE 1
 REDSHIFT AND OPTICAL LUMINOSITY DATA FOR INTRINSICALLY BRIGHT SPIRALS OF HUBBLE TYPE Sc, Sbc, AND Sb

Galaxy (1)	Type (2)	v_0^{220} (km s ⁻¹) (3)	Δv_0^{220} (4)	$\log v_0^{220}$ (5)	B_T (6)	$B_T^{o,i}$ (7)	$-M_{gr}^o$ (RSA) (8)	$-M_{gr}^{o,i}$ (RSA) (9)	$-M_{gr}^{o,i}$ (220) (10)
{Sbc, SBbc} {I-I.3}									
NGC 309	Sc(r)I	5786	-180	3.748	12.40	12.07	22.92	23.25	23.17
521	SBc(rs)I	5223	-161	3.704	12.5	12.19	22.57	22.88	22.83
628	Sc(s)I	861	-42	2.913	9.77	9.43	21.44	21.75	21.64
958	Sc(s)I.2	5837	-137	3.756	12.95	12.32	22.39	23.03	22.97
1232	Sc(rs)I	1775	-63	3.233	10.50	10.18	22.25	22.57	22.49
1376	Sc(s)I	4198	-96	3.613	12.79	12.43	21.89	22.19	22.14
2207	Sc(s)I.2	2590	63	3.424	11.35	10.60	22.54	22.97	23.02
2280	Sc(s)I.2	1709	103	3.258	11.96	11.04	21.14	21.63	21.75
2776	Sc(rs)I	2673	247	3.466	12.20	11.84	21.50	21.80	21.99
2835	SBc(rs)I.2	624	151	2.889	10.95	10.25	20.23	19.81	20.70
2942	Sc(s)I.3	4399	236	3.666	12.79	12.39	21.97	22.33	22.44
2955	Sc(s)I	7051	201	3.860	13.45	12.90	22.34	22.85	22.90
2989	Sc(s)I	3916	222	3.617	12.42	12.87	21.22	21.60	21.72
2997	Sc(s)I.3	799	196	2.998	10.32	9.62	21.03	21.40	21.87
2998	Sc(rs)I	4813	221	3.702	12.65	12.08	22.30	22.84	22.93
3294	Sc(s)I.3	1566	356	3.284	12.2	11.69	20.28	20.79	21.23
3464	Sc(rs)I	3571	263	3.584	12.82	12.31	21.55	21.96	22.11
3478	Sc(s)I	6730	217	3.842	12.95	12.38	22.70	23.27	23.33
3614	Sc(r)I	2362	321	3.429	12.21	11.75	21.16	21.62	21.90
3735	Sc(s)I	2836	220	3.486	12.50	11.62	21.32	22.15	22.31
3893	Sc(s)I.2	1026	305	3.125	11.1	10.65	20.46	20.91	21.48
3938	Sc(s)I	844	214	3.025	10.91	10.60	20.23	20.54	21.03
IC 764	Sc(s)I.2	1851	320	3.337	12.35	11.24	20.61	21.60	21.95
4254	Sc(s)I.3	2301	Virgo	3.074	10.43	10.11	21.27	21.59	21.76
4303	Sc(s)I.2	1404	Virgo	3.074	10.17	9.86	21.53	21.84	22.01
4321	ScI	1464	Virgo	3.074	10.11	9.79	21.59	21.91	22.08
4535	SBc(s)I.3	1818	Virgo	3.074	10.51	10.12	21.19	21.58	22.15
4653	Sc(rs)I.3	2433	384	3.450	12.82	12.51	20.62	20.93	21.24
5161	Sc(s)I	2113	290	3.381	11.98	11.24	21.32	21.92	22.17
5230	Sc(s)I	6755	256	3.846	12.75	12.43	22.90	23.22	23.30
5364	Sc(r)I	1140	425	3.195	11.05	10.64	20.74	21.15	21.84
5457	Sc(s)I	M101Grp	22	2.460	8.18	7.89	21.22	21.31	20.91
5660	Sc(s)I.2	2433	296	3.436	12.3	11.99	21.14	21.45	21.69
6118	Sc(s)I.3	1535	250	3.252	11.91	11.24	20.65	21.20	21.52
6878	Sc(r)I.3	5791	-57	3.758	14.07	13.58	21.36	21.74	21.71
2120-46	Sc(s)I	2600	-48	3.407	12.56	11.78	21.07	21.80	21.76
{Sbc, SBbc} {I-I.3}									
NGC 1241	SBbc(rs)I.2	4072	-115	3.597	12.66	12.21	21.89	22.34	22.51
1365	SBbc(s)I	1486	-32	3.163	10.21	9.45	22.19	22.95	22.87
1566	Sbc(s)I.2	1303	18	3.121	10.21	9.79	21.91	22.27	22.32
2223	SBbc(r)I.3	2529	72	3.415	12.15	11.48	21.72	22.04	22.10
2336	SBbc(r)I	2424	165	3.413	11.12	10.48	22.45	22.94	23.09
2369	Sbc(s)Ipec	3016	64	3.488	12.68	11.77	21.46	22.13	22.17
2713	Sbc(s)I	3690	226	3.593	12.60	11.87	21.88	22.47	22.60
3054	SBbc(s)I	1923	268	3.341	12.13	11.47	21.02	21.46	21.97
3124	SBbc(r)I	3307	254	3.552	12.35	11.87	21.89	22.23	22.39
3145	SBbc(rs)I	3416	265	3.566	12.35	11.73	21.92	22.44	22.60
3259	Sbc(r)I	2005	256	3.355	12.91	12.12	20.17	20.91	21.16
3344	Sbc(rs)I.2	627	19	2.811	10.48	10.14	20.01	20.35	20.42
3433	Sbc(r)I.3	2566	353	3.465	12.28	11.97	21.27	21.58	21.86
3486	Sbc(r)I.2	636	10	2.811	10.85	10.47	19.67	20.05	20.09
3687	SBbc(r)I.2	2456	362	3.450	12.85	12.57	20.59	20.89	21.31
3720	Sbc(s)I	5831	264	3.785	13.70	13.39	21.63	21.94	22.03
3963	Sbc(r)I.2	3295	254	3.550	12.38	12.07	21.71	22.02	22.18
4030	Sbc(r)I	1322	474	3.255	11.07	10.69	21.04	21.42	22.09
4939	Sbc(rs)I	2903	332	3.510	11.56	11.05	22.26	22.77	23.00
5324	Sbc(r)I.3	2853	330	3.503	12.43	12.14	21.35	21.64	21.88
5351	Sbc(rs)I.2	3663	291	3.597	13.00	12.25	21.32	22.07	22.24
5426	Sbc(rs)I.2	2455	343	3.447	12.78	12.28	20.68	21.18	21.46
5427	Sbc(s)I	2565	335	3.463	12.07	11.76	21.48	21.79	22.05
5905	SBbc(rs)I	3544	225	3.576	12.33	11.77	21.92	22.48	22.61
6699	Sbc(s)I.2	3357	26	3.529	12.73	12.22	21.62	21.92	21.93

TABLE 1—Continued

Galaxy (1)	Type (2)	v_0^{220} (km s $^{-1}$) (3)	Δv_0^{220} (4)	$\log v_0^{220}$ (5)	B_T (6)	B_T^i (7)	$-M_{Br}^0$ (RSA) (8)	$-M_{Br}^i$ (RSA) (9)	$-M_{Br}^i$ (220) (10)
{Sbc, SBbc}									
{I-II}									
IC 214	Sbc(r)I-II	4757	-121	3.666	12.95	12.48	22.03	22.41	22.35
289	SBbc(rs)I-II	1834	-100	3.239	11.81	11.41	21.01	21.41	21.51
1788	Sbc(s)I-II	3366	-116	3.512	13.10	12.53	21.04	21.61	21.53
976	Sbc(r)I-II	4550	-99	3.648	13.21	12.79	21.68	22.01	21.85
1097	R SBbc(rs)I-II	1284	-52	3.090	10.16	9.75	21.89	22.30	22.20
1625	Sbc(s)I-II	3032	-23	3.478	13.2	12.32	20.83	21.59	21.57
1640	SBbc(r)I-II	1600	6	3.205	12.45	11.96	20.17	20.57	20.57
2347	Sbc(r)I-II	4692	126	3.683	13.30	12.54	21.72	22.32	22.38
2545	SBbc(r)I-II	3312	196	3.545	13.20	12.57	21.07	21.54	21.66
3001	SBbc(s)I-II	2171	241	3.382	12.72	11.99	20.78	21.20	21.42
3162	Sbc(s)I.8	1226	356	3.199	12.15	11.82	19.80	20.13	20.68
3338	Sbc(s)I-II	1171	398	3.196	11.32	10.89	20.53	20.96	21.59
3430	Sbc(rs)I-II	1555	383	3.288	12.15	11.68	20.31	20.78	21.26
3506	Sbc(s)I-II	6348	257	3.820	13.44	12.97	22.08	22.55	22.63
3953	SBbc(r)I-II	1036	295	3.124	10.79	10.28	20.79	21.30	21.84
3981	Sbc(s)I-II	1554	368	3.284	12.44	11.39	20.09	21.07	21.53
4045	Sbc(s)I-II	1765	442	3.344	12.65	12.26	20.09	20.48	20.96
4123	SBbc(rs)I.8	1159	517	3.224	11.84	11.47	19.99	20.36	21.15
4412	SBbc(s)I-IIpec	1577	Virgo	3.074	13.07	12.76	19.42	19.73	19.11
4603	Sbc(s)I-II	2073	267	3.369	12.09	11.43	21.22	21.66	21.92
4891	SBbc(r)I-II	2418	351	3.442	12.61	12.25	20.85	21.17	21.65
4947	Sbc(s)I-IIpec	2222	281	3.399	12.74	12.11	20.65	21.13	21.39
5194	Sbc(s)I-II	541	52	2.774	8.98	8.57	21.24	21.65	21.80
5248	Sbc(s)I-II	1049	468	3.182	10.80	10.42	20.81	21.19	21.99
5350	SBbc(rs)I-II	2305	337	3.422	12.2	11.84	21.12	21.48	21.77
5430	SBbc(s)I.8	3016	251	2.514	12.78	12.10	21.12	21.80	21.97
5592	Sbc(s)I-II	4190	225	3.645	13.27	12.74	21.48	21.88	21.99
5921	SBbc(s)I-II	1428	323	3.244	11.53	11.14	20.80	21.14	21.58
6780	Sbc(rs)I-II	3381	8	3.530	13.15	12.64	21.16	21.51	21.51
6814	Sbc(rs)I-II	1643	43	3.227	12.02	11.37	20.91	21.21	21.27
6925	Sbc(r)I-II	2780	-35	3.438	12.10	11.36	21.73	22.37	22.33
6984	Sbc(r)I.8	4435	-60	3.641	13.33	12.84	21.48	21.90	21.87
7038	Sbc(s)I.8	4785	-80	3.672	12.36	11.84	22.60	23.06	23.02
7124	Sbc(rs)I-II	4957	-87	3.687	13.10	12.48	21.92	22.50	22.46
7171	Sbc(r)I-II	2758	-95	3.425	13.00	12.25	20.76	21.46	21.38
7392	Sbc(s)I-II	3035	-124	3.464	12.65	12.19	21.27	21.73	21.63
7479	SBbc(s)I-II	2630	-98	3.403	11.7	11.27	21.97	22.34	22.25
7531	Sbc(r)I-II	1607	-62	3.188	12.14	11.54	20.40	21.00	21.23
7678	SBbc(s)I-II	3756	-109	3.562	12.8	12.33	21.67	22.05	21.98
7755	SBbc(r)/Sbc(r)I-II	2969	-119	3.455	12.10	11.73	21.77	22.14	22.05
{Sb, SBb}									
{I-I.3}									
NGC 210	Sb(rs)I	1875	-115	3.246	11.65	11.01	21.22	21.86	21.72
772	Sb(rs)I	2645	-93	3.407	11.10	10.33	22.59	23.29	23.20
1300	SB(s)I.2	1526	-53	3.168	11.10	10.43	21.32	21.99	21.91
1417	Sb(s)I.3	4139	-93	3.607	12.75	12.02	21.90	22.57	22.52
1512	SBb(rs)Ipec	760	12	2.888	11.38	10.77	19.58	20.14	20.17
1832	SBb(r)I	1855	24	3.274	12.1	11.32	20.89	21.53	21.55
2523	SBb(r)I	3638	157	3.579	12.65	11.86	21.78	22.45	22.54
2633	SBb(s)I.3	2416	189	3.416	12.85	12.09	20.67	21.33	21.49
2935	SBb(s)I.2	2003	264	3.355	12.00	11.25	21.22	21.76	22.03
3200	Sb(r)I	3313	260	3.553	12.29	11.16	21.94	22.95	23.11
3347	SBb(r)I	2626	243	3.458	12.27	11.29	21.59	22.31	22.50
3642	Sb(r)I	1733	297	3.308	11.53	11.01	21.17	21.69	22.03
3992	SBb(rs)I	1134	310	3.159	10.64	9.95	21.14	21.83	22.35
4814	Sb(s)I	2650	276	3.466	12.8	12.21	20.82	21.41	21.41
4999	SBb(rs)I	2954	350	3.519	12.64	12.12	21.22	21.74	21.98
5033	Sb(s)I	897	249	3.059	10.63	10.11	20.64	21.16	21.69
5172	SbI	3960	309	3.630	12.60	11.85	21.89	22.64	22.81
5371	Sb(rs)I/SBb(rs)I	2616	320	3.468	11.40	10.81	22.19	22.78	23.03
5406	SBb(r)I	5241	252	3.740	12.96	12.58	22.14	22.52	22.62
5533	Sb(s)I	3903	277	3.621	12.65	11.98	21.81	22.48	22.63
5792	SBb(s)I.3	1889	332	3.347	11.72	10.54	21.21	22.35	22.70
5878	Sb(s)I.2	1974	291	3.355	12.3	11.35	20.77	21.63	21.93
5985	SBb(r)I	2694	225	3.465	11.80	11.01	21.90	22.64	22.82
6384	Sb(r)I.2	1735	182	3.283	11.29	10.42	21.65	22.28	22.50
6753	Sb(r)I	3001	23	3.481	11.93	11.25	22.14	22.64	22.65
6951	Sb/SBb(rs)I.3	710	113	3.261	12.2	11.31	20.85	21.36	21.50
7606	Sb(r)I	2323	-120	3.343	11.55	10.65	21.79	22.69	22.57

TABLE 1—Continued

Galaxy (1)	Type (2)	v_0^{220} (km s ⁻¹) (3)	Δv_0^{220} (4)	$\log v_0^{220}$ (5)	B_T (6)	$B_T^{2,i}$ (7)	$-M_{Br}^0$ (RSA) (8)	$-M_{Br}^{0,i}$ (RSA) (9)	$-M_{Br}^{0,i}$ (220) (10)
{Sb, SBb} {I-II}									
NGC 23	SbI-II	4836	-119	3.674	12.80	12.07	22.22	22.86	22.80
224	SbI-II	4.38	2.71	20.50	21.53	21.53
615	Sb(r)I-II	1971	-106	3.271	12.3	11.39	20.68	21.59	21.46
670	Sb(s)I-II	4023	-94	3.594	13.17	12.19	21.47	22.34	22.28
779	Sb(rs)I-II	1492	-83	3.149	11.86	10.80	20.51	21.57	21.45
782	SBb(r)I-II	5881	-97	3.762	12.83	12.36	22.52	22.99	22.95
986	SBb(rs)I-II	2006	-73	3.286	11.8	11.21	21.22	21.81	21.72
1228	Sb(r)I-II	4461	-104	3.639	12.80	12.33	21.95	22.42	22.37
1433	SBb(s)I-II	923	4	2.967	10.68	10.18	20.65	21.15	21.16
1964	Sb(s)I-II	1579	49	3.212	11.60	10.49	21.06	22.01	22.07
2551	Sb(r)I-II	2484	182	3.426	13.05	12.31	20.54	21.17	21.32
2642	SBb(rs)I-II	4262	185	3.648	12.54	11.88	21.33	21.77	22.86
2712	SBb(s)I-II	1892	263	3.333	12.70	11.89	20.26	21.00	21.28
2815	Sb(s)I-II	2333	231	3.409	12.66	11.34	20.99	22.00	22.21
3031	Sb(r)I-II	7.86	7.01	21.01	21.79	21.79
3147	Sb(s)I.8	2899	197	3.491	11.45	10.88	22.44	22.94	23.08
3169	Sb(r)I-II	1067	327	3.144	11.28	10.56	20.42	21.09	21.66
3223	Sb(s)I-II	2619	238	3.456	11.88	10.91	21.98	22.69	22.87
3504	Sb(s)/SBb(s)I-II	1480	410	3.276	11.8	11.25	20.56	21.11	21.64
3673	Sb(s)I-II	1662	315	3.298	12.41	11.65	20.32	20.96	21.34
3681	SBb(r)I-II	1135	477	3.207	12.40	11.94	19.38	19.84	20.60
3705	Sb(r)I-II	870	-46	2.916	11.77	10.88	19.43	20.32	20.20
4050	Sb(r)I-II	1661	383	3.310	12.25	11.58	20.41	21.03	21.48
4394	SBb(sr)I-II	853	Virgo	3.074	11.76	11.28	20.94	21.42	20.59
4548	SBb(rs)I-II	366	Virgo	3.074	10.98	10.43	20.72	21.27	21.44
4593	SBb(rs)I-II	2505	368	3.458	11.72	11.15	21.78	22.35	22.64
4679	Sb(s)I-II	4509	211	3.674	12.95	12.23	22.03	22.55	22.64
4902	SBb(s)I-II	2426	347	3.443	11.90	11.39	21.57	22.04	22.33
5054	Sb(s)I-II	1524	380	3.280	11.51	10.75	20.98	21.69	22.15
5150	Sb(r)I-II	4127	241	2.640	13.26	12.72	21.43	21.86	21.98
5156	SBb(rs)I-II	2670	212	2.460	12.87	12.15	21.20	21.55	21.65
IC 4351	Sb(s)I-II	2367	284	3.423	12.30	10.86	21.23	22.55	22.76
5347	SBb(s)I-II	2394	348	3.438	13.40	12.86	20.00	20.54	20.83
5740	Sb(s)I-II	1490	362	3.268	12.62	11.86	19.75	20.51	20.98
5850	SBb(sr)I-II	2430	304	3.437	11.71	11.20	21.76	22.23	22.49
6887	Sb(s)I-II	2938	-17	3.465	12.46	11.43	21.49	22.42	22.40
7083	Sb(s)I-II	2951	-30	3.466	11.80	11.04	22.12	22.81	22.78
7329	SBb(r)I-II	3043	-39	3.478	12.32	11.84	21.65	22.08	22.28
7331	Sb(rs)I-II	1114	1	3.047	10.39	9.14	21.59	22.60	22.60
7552	SBb(s)I-II	1565	-67	3.176	11.40	10.99	21.08	21.49	21.39
7723	SBb(rs)I-II	1976	-111	3.271	11.85	11.23	21.13	21.75	21.62
7782	Sb(s)I-II	5584	-158	3.734	13.1	12.36	22.14	22.88	22.81

ations from the Hubble flow. Redshifts, 21 cm line widths, and magnitudes are listed for these galaxies between $m \sim 14$ and $m \sim 15$ in their original paper.

The data for the S-T sample are listed in Table 2. The galaxy name is in column (1); identification data can be found in the original catalog (ST 1975b). Columns (2), (3), and (5) list m_{pg} magnitudes (based on the Zwicky *et al.* 1961/68 catalogs), axial ratios a/b , and redshifts relative to the Local Group centroid. The magnitudes⁴ in column (4) are the column (2) values corrected for galactic and internal absorption, the latter adopted from the RSA to be $A^i = 0.28 + 0.88 \log a/b$ for this type of galaxy.

The B_T , $\log v_0$ Hubble diagrams for the bright RSA spirals with both the S-T and the Rubin faint samples added are shown in Figure 5. Only the RSA spirals of type Sb, Sbc, and Sc of luminosity class I-1.3 are plotted. The total S-T sample is added in Figure 5a. The subset of the Rubin sample that is

restricted to their type I to I.3 is plotted in Figure 5b. The envelope and ridge lines are drawn with a slope of 5.

The bias effect is again seen in each plot, but now with a most interesting difference. As in Figures 2 and 3, the slope of the RSA sample alone is again less than 5, but the slope of the fainter sample alone (open circles for the S-T sample and triangles for the Rubin) is also less than 5, i.e., there is a different distribution of points between the envelope lines for the bright compared with the faint samples. This is because each shows the Malmquist bias separately (each being flux-limited samples), but the bias starts at different magnitudes. This, of course, is the expected behavior if method (1) is correct as seen from Figure 6 where least-squares regressions are put separately through the RSA and the fainter S-T sample, taking the residuals as magnitude differences. The discontinuity between the two samples in Figure 6 can be understood from the bias diagram of Figure 7, similar to Figures 1a and 4a but now with the faint S-T sample added in Figure 7b. This discontinuity would not be present if the velocity field were nonlinear,

⁴ See page 591.

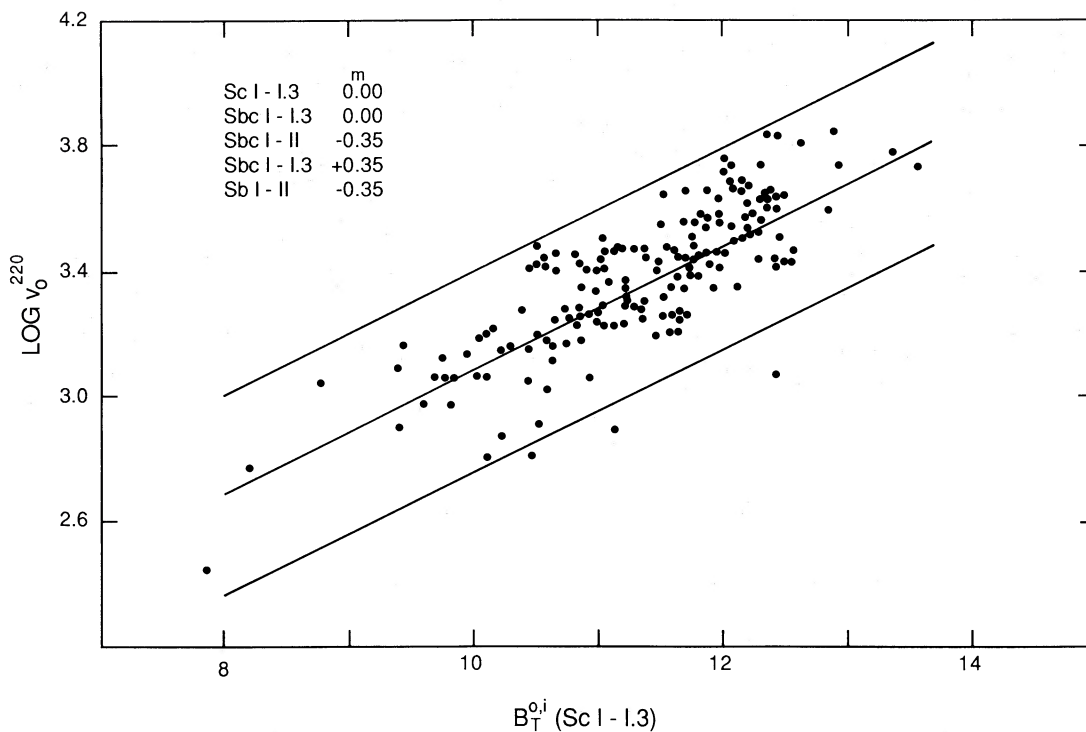


FIG. 2.—The magnitude-redshift diagram for Sb and Sc galaxies of the brightest luminosity classes that are contained in the RSA catalog. Galaxies with Hubble types and van den Bergh luminosity classes that differ from those of ScI-1.3 are reduced to that absolute magnitude system by the corrections shown in the code, found from the data in Table 1. The ridge and envelope lines are drawn with a slope of 5.

⁴ The m_{pg} magnitudes in column (2) are those listed by S-T in their Table 4, column (3). They are based on the Zwicky *et al.* (1961/68) magnitudes, corrected for a mean zero point difference of $m_{pg} - m_{zw} = -0.1$, applied independent of the diameter. This correction was determined by S-T from their aperture photometry of 11 galaxies fainter than $m_{zw} = 13.8$ (ST 1975a, Table 3). The S-T photoelectric values were reduced to the HMS (1956, Appendix A) m_{pg} system, which is the same to within 0.04 ± 0.2 mag as the zero point of the Holmberg (1958) system (HMS, Figure A5). In turn, the Holmberg zero point differs by 0.12 mag from B_T for Holmberg colors of $C = 0.5$ in the sense of B_T being fainter than m_{H_0} (Table 11 of the RC2).

If this were the correct reduction of m_{zw} magnitudes to the B_T system, then the m_{pg} values in column (2) of Table 2 would be 0.12 mag brighter than the RC2 B_T values in Table 1 here. However, Graham's (1976) photometry shows a stronger aperture effect, consistent in sign with what was known before (ST, 1975b; § IIIb) but very much larger in amplitude, giving corrections that range from $\Delta m = B_T - m_{zw} = -0.9$ to $+0.9$ mag for the Table 2 galaxies, depending on the estimated diameters. These magnitude corrections depend critically on the diameter values, which are quite uncertain, making this route to the conversion of m_{zw} to B_T untenable at present.

Indeed, comparison of the Table 2 m_{pg} values with B_T determined from the photoelectric aperture photometry of Bothun *et al.* (1984, Table 2) as reduced to the RC2 system by the referee, gives a correction of $\langle B_T - m_{pg} \rangle = -0.3 \pm 0.1$. But even this correction is small compared with the intrinsic scatter in Figures 5a, 6, 7, 10, and 12. More importantly, it is negligible for the proof given in Figure 7 that the fainter S-T sample and the Rubin *et al.* sample (Figures 8 and 9 here) fill the $M, \log v$ diagram, as expected if the $\langle M \rangle = f(D)$ correlation of Figure 4a is due to the flux-biased RSA sample. To destroy the proof would require a mean magnitude correction far in excess of any of the suggested small corrections discussed above and/or a gross misidentification of ScI type galaxies toward later luminosity classes for the faint galaxy samples used here (see footnote 5). Because the magnitudes of the faint galaxies are used only for qualitative tests for bias in the remainder of the paper, we make no distinction in the following diagrams between B_T and the m_{pg} values that are listed either by S-T or by Rubin *et al.* (1976), because the magnitude corrections to B_T are, themselves, small.

according to the argument given in § II and shown later in § IV (Figs. 11 and 12) because the triangles in Figure 7b would not fill the space between the two limit lines but would tack on smoothly to the distribution shown by the closed circles.

Instead, what we see in Figure 7b is the filling out of the Figure 1a $\Phi(M)$ distribution with what is becoming an approximate distance-limited sample, now complete to $\log v_0 \sim 3.5$ rather than only ~ 3.0 as in Figure 4, for the RSA sample. That the triangles in Figure 7b do not abut smoothly onto the upper part of the distribution of the circles near $\log v \sim 3.7$ is one of the two proofs that the results of using method (2) are wrong. For the other we now follow method (2) to reach a contradiction.

IV. A MULTIVALUED HUBBLE CONSTANT OBTAINED BY APPLYING A FIXED $\langle M \rangle$ TO EACH DATA SAMPLE SEPARATELY

The steps for method (2) have been given in § IIb. We have applied the method to the three ScI data lists set out in the previous sections. For definiteness $\langle M_{B_T}^{0,i} \rangle$ was adopted as -21.2 , to be adjusted later (§ VI) using the local calibrations of M31, M81, and M101.

It is clear from Figures 1b, 4a, and 7a that if we require $\langle M \rangle$ to be constant for the sample, the $h_i = v_i/r_i = v_i/\text{dex} [0.2(m_i - \langle M \rangle + 5)]$ must vary with v_i . Figure 8a shows the result of calculating h_i for galaxies in Table 1 of the types indicated. We have simply reproduced here results similar to those shown by de Vaucouleurs (1972), by de Vaucouleurs and Peters (1986, their Figs. 2a and 2b), and by Giraud (1986a, Fig. 1; 1986b, Figs. 4 etc.), and explained as bias by Teerikorpi (1975a, b, 1984), STY (1979), TYS (1979), and Bottinelli *et al.* (1986).

The mean $\langle h_i \rangle$ values vary from ~ 35 to $90 \text{ km s}^{-1} \text{ Mpc}^{-1}$ in Figure 8a over the redshift range from 1000 km s^{-1} to 7000 km s^{-1} . If this variation were to be real, the fainter ScI

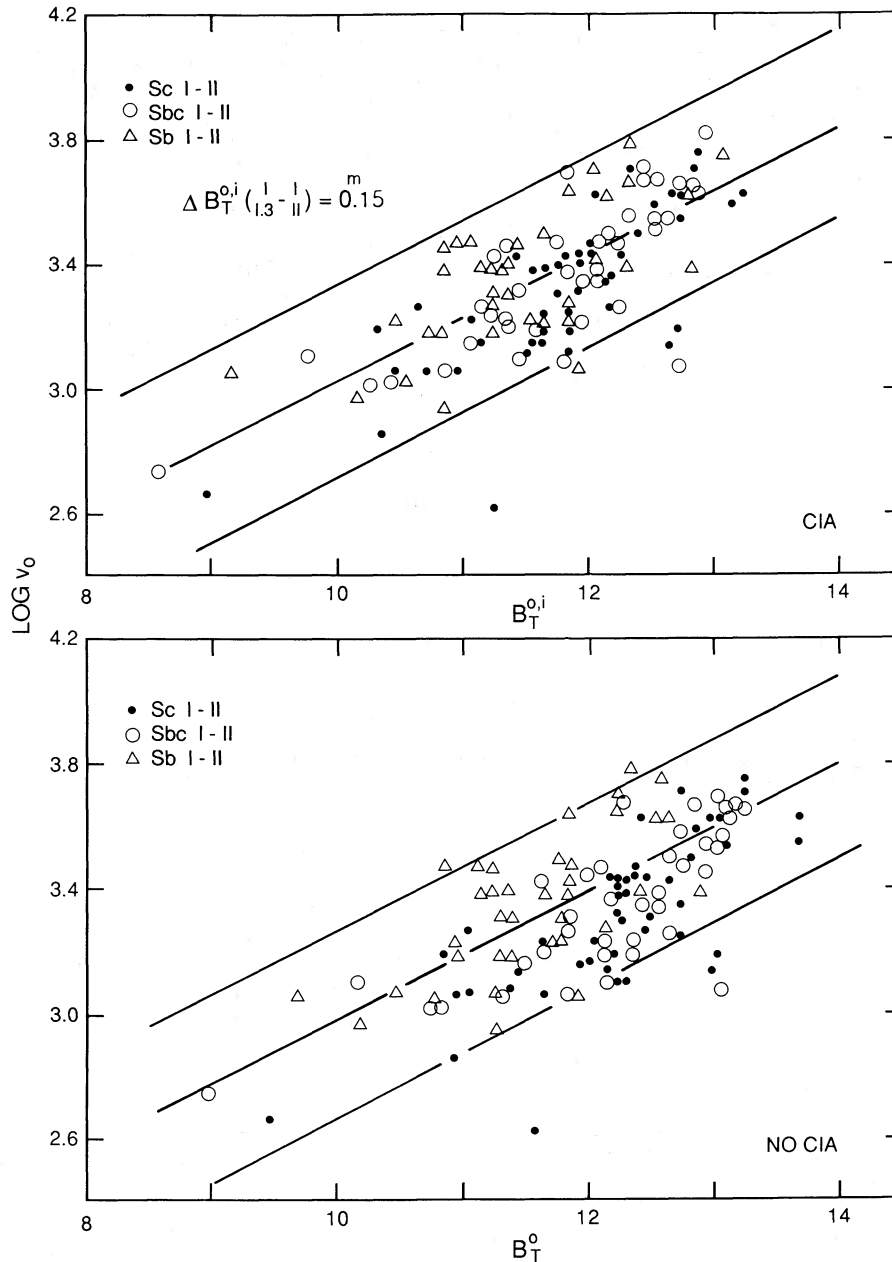


FIG. 3.—The magnitude-redshift diagram for Sb and Sc galaxies of lower luminosity class than in Fig. 2. Top panel shows the correlation using fully corrected magnitudes $B_T^{o,i}$. The mean magnitude difference between the data here from those in Fig. 2 is $\Delta B_T^{o,i} = 0.15$; the data here being fainter. The bottom panel shows the correlation without the magnitude correction for internal absorption.

samples must give the same values of h_i at any given common redshift. Figure 8b shows the calculation using the S-T faint sample of Table 2. The mean regression through the points of Figure 8a is shown as a solid line.

The data points for the faint S-T sample, in Figure 8b, again show a variation of $\langle h_i \rangle$ over the same range from ~ 30 to 100 but now displaced toward larger velocities. Said differently, the effective Hubble constant h_i found by using method (2) is multi-valued at a given redshift—clearly a contradiction. The same is shown in Figure 8c from the Rubin *et al.* sample.⁵

What, in fact, we are seeing in Figure 8 is a proper filling out of the h_i , v_i plane using a total sample that approaches a volume limited set for $v \lesssim 3000 \text{ km s}^{-1}$. This is similar to the

⁵ The validity of the argument of why adding the faint sample in Figure 7b gives a direct demonstration of the bias, and why method (2) gives a multi-valued Hubble constant in Figure 8 depends on the supposition that the faint galaxies we have added are ScI types, similar in their relevant properties with the bright RSA galaxies listed in Table 1. The question was discussed by S-T (1975b) in their § V, listing six points in support of this supposition. Furthermore, the experiment they performed on the effect of reduced spatial resolution of faint galaxies relative to the RSA sample was conclusive in showing that remote ScI galaxies at $v \sim 10,000 \text{ km s}^{-1}$ could be recognized on the POSS (S-T 1975b, § II) plates. The experiment consisted of inspecting selected nearby galaxies from Table 1 on the *Lick Observatory Sky Atlas* prints whose scale for these bright ScI galaxies matched the much larger focal length scale of the POSS from which the remote ScI sample was chosen. This is the same resolution test that was made later by Rubin *et al.* (1976), with the same conclusion that the galaxies in the faint sample are predominantly SbI and ScI types with very little confusion as to the morphological classification.

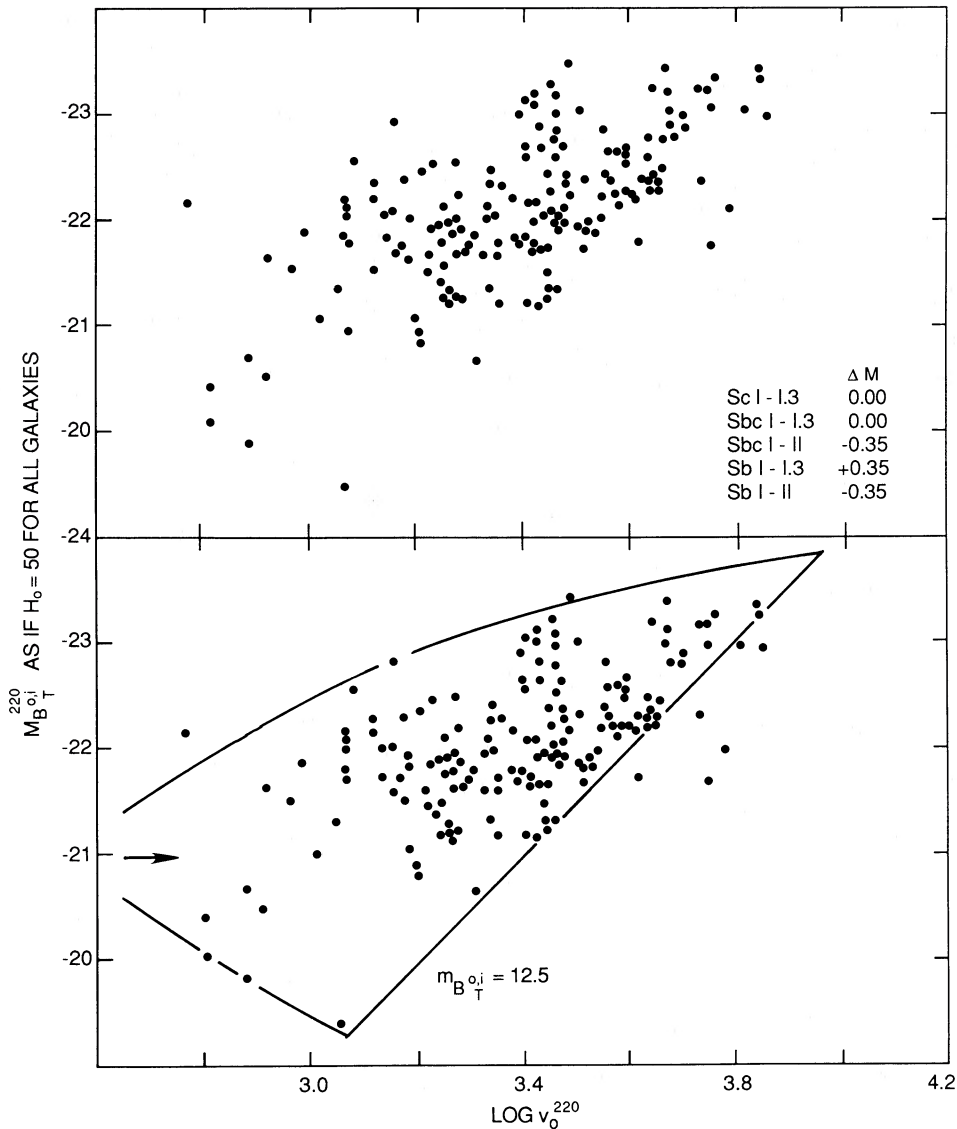


FIG. 4.—*Top*: The apparent variation of the absolute magnitude $M_{B_T}^{o,i}$ with redshift for the RSA sample of Sb to Sc galaxies of bright luminosity class, reduced to the magnitude system of the ScI-I.3 sample by the corrections shown in the code. *Bottom*: Same as the top panel but with envelope lines and the $m = 12.5$ flux limit line superposed. The apparent increase in mean luminosity with distance is an artifact of the flux limitation of the sample.

effect seen in Figures 4*b* and 7*b* in the different representation of the same result. This is shown more clearly in Figure 9 where the separate samples of Figure 8 have been combined. The top panel is the same as Figure 8*a* but with the $m = 13$ limit line of the RSA shown, and with an upper envelope line drawn by eye to accommodate most of the data. The beginning of a lower envelope is shown, truncated at $v \sim 2000 \text{ km s}^{-1}$ by the $m = 13$ limit line. Figure 9*b* shows the S-T sample added from Figure 8*b*, now with a $m = 15.5$ limit line drawn that truncates the lower envelope at $v \sim 5000 \text{ km s}^{-1}$. The same for the Rubin *et al.* sample is shown in Figure 9*c*.

The sum of the top three panels is in Figure 9*d* which contains the principal conclusion. The h_i, v_i plane is filled in a more proper way as the sample approaches a volume-limited set, showing that the apparent variation of h_i with v_i using RSA sample alone is not real. To the extent that the statistics of the present ScI total sample approximates a proper volume-limited set,⁶ the mean Hubble constant from these data is

$\langle \text{dex} [\log h_i] \sim 50 \text{ km s}^{-1} \text{ Mpc}^{-1} \text{ if } \langle M_{B_T}^{o,i} \rangle = -21.2 \text{ for the set. The correct value of } \langle M_{B_T}^{o,i} \rangle \text{ to use is the subject of } \S \text{ VI where data for M31, M81, and M101 are applied to obtain a direct calibration of } \langle M \rangle \text{ and therefrom a proper value for } H_0.$

⁶ The distribution of points in Figures 7*b*, 9, and later in Figures 10 and 12 is not uniform, showing gaps between the bright and faint samples. This is most likely due to the incompleteness of the RSA near its flux limit of $m \sim 13$ (STY 1979, Fig. 6), and even greater incompleteness of the two faint surveys, especially near their bright boundary between $m_{pg} \sim 13$ to 14. These discontinuities are especially visible in Figures 10 and 12. It is for this reason that we prefer the upper and lower boundary argument of the next section to estimate $M_{B_T}(\text{apex})$ rather than an analysis of the distribution of points within the boundary lines.

Figure 9 with its upper and lower envelope lines and the flux cutoff lines is similar to Figure 9 of de Vaucouleurs and Bollinger (1979), but with a different conclusion drawn here as to the meaning of the apparent increase of H_0 with redshift for the incomplete sample that is flux-limited. The similarity of the two diagrams, but their different interpretation, was recalled by de Vaucouleurs as a helpful comment on an early draft of this paper.

TABLE 2
MAGNITUDE AND REDSHIFT DATA FOR THE FAINT S-T SCl GALAXY SAMPLE

Name (1)	m_{pg} (2)	a/b (3)	$m_{pg}^{o,i}$ (4)	v_0 (km s $^{-1}$) (5)	$\log v_0$ (6)	M_{pg}^o ($H_0 = 50$) (7)	$M_{pg}^{o,i}$ ($H_0 = 50$) (8)
NGC 7816	13.90	1.23	13.54	5285	3.723	-21.22	-21.58
0008+02	15.54	1.56	15.09	12874	4.110	-21.52	-21.97
NGC 36	14.40	2.11	13.83	6241	3.795	-21.08	-21.65
NGC 99	13.90	1.04	13.60	5343	3.728	-21.25	-21.55
NGC 105	14.00	1.33	13.61	5439	3.736	-21.19	-21.58
0028+13	15.20	1.35	14.80	10081	4.004	-21.33	-21.73
0033+12	15.20	1.04	14.90	10205	4.009	-21.35	-21.65
NGC 173	14.40	1.35	14.00	4332	3.637	-20.29	-20.69
NGC 180	14.20	1.38	13.80	5377	3.731	-20.96	-21.36
NGC 182	13.70	1.59	13.24	5363	3.729	-21.45	-21.91
0037+02	(13.7)	2.18	13.12	5244	3.720	-21.41	-21.99
NGC 257	13.60	1.56	13.15	5420	3.734	-21.58	-22.03
0054-01	15.20	1.18	14.86	15124	4.180	-22.21	-22.55
0112-00	14.40	1.00	14.12	10209	4.009	-22.15	-22.43
0115+11	14.20	1.60	13.74	5170	3.713	-20.87	-21.33
0116+01	15.67	1.14	15.34	13412	4.127	-21.47	-21.80
0117+07	14.80	1.05	14.50	9564	3.981	-21.61	-21.91
NGC 497	14.00	2.34	13.40	8176	3.913	-22.07	-22.67
NGC 521	12.80	1.00	12.52	5100	3.708	-22.25	-22.53
IC 1706	14.10	1.33	13.71	6461	3.810	-21.46	-21.85
0135+07	14.70	1.42	14.29	4307	3.634	-19.98	-20.39
NGC 658	13.50	2.08	12.94	3078	3.488	-20.45	-21.01
NGC 664	13.80	1.30	13.42	5473	3.738	-21.40	-21.78
NGC 673	13.20	1.36	12.80	5326	3.726	-21.94	-22.34
0145+12	13.90	1.25	13.54	5383	3.731	-21.26	-21.62
NGC 706	13.10	1.50	12.66	4974	3.697	-21.89	-22.33
IC 1743	13.90	2.19	13.32	4646	3.667	-20.94	-21.52
0152+06	14.40	1.29	14.02	5251	3.720	-20.71	-21.09
IC 173	14.80	1.42	14.39	13947	4.144	-22.43	-22.84
0158+08	14.30	2.00	13.76	4819	3.683	-20.62	-21.16
IC 198	14.70	2.10	14.14	9476	3.977	-21.69	-22.25
NGC 840	14.60	2.34	14.00	7196	3.857	-21.19	-21.79
IC 211	14.40	1.52	13.96	3355	3.526	-19.74	-20.18
NGC 926	13.80	2.57	13.16	6510	3.814	-21.78	-22.42
0228+01	14.50	1.82	13.99	7407	3.870	-21.36	-21.87
0229-01	14.20	1.59	13.74	11268	4.052	-22.57	-23.03
NGC 1019	14.50	1.29	14.12	7258	3.861	-21.31	-21.69
NGC 1085	13.50	1.23	13.14	6986	3.844	-22.23	-22.59
NGC 1094	13.40	1.50	12.96	6284	3.798	-22.10	-22.54
0950+43	14.40	1.06	14.10	4798	3.681	-20.51	-20.81
1001+14	15.10	1.07	14.79	8828	3.946	-21.14	-21.45
1001+13	13.50	1.25	13.13	2577	3.411	-20.06	-20.43
1002+51	15.67	1.43	15.25	14092	4.149	-21.58	-22.00
1012+55	14.50	1.24	14.14	7301	3.863	-21.32	-21.68
1013+05	14.50	1.85	13.98	13586	4.133	-22.67	-23.19
1014+53	15.20	1.23	14.84	13658	4.135	-21.98	-22.34
NGC 3191	13.80	1.50	13.36	9146	3.961	-22.51	-22.95
NGC 3202	14.10	1.26	13.73	6729	3.828	-21.55	-21.92
1022+55	15.00	1.13	14.67	7669	3.885	-20.93	-21.26
NGC 3408	14.00	1.00	13.72	9670	3.985	-22.43	-22.71
1049+59	14.80	1.43	14.38	8489	3.929	-21.35	-21.77
1051+56	15.67	1.36	15.27	14575	4.164	-21.66	-22.06
NGC 3470	14.20	1.06	13.90	6737	3.828	-21.45	-21.75
1103+57	14.90	1.16	14.56	9886	3.995	-21.58	-21.92
1111+57	15.20	1.25	14.83	10079	4.003	-21.32	-21.69
1111+56	15.54	1.29	15.16	10432	4.018	-21.06	-21.44
NGC 7428	13.70	1.85	13.18	3195	3.504	-20.33	-20.85
2255+02	14.80	1.07	14.49	4955	3.695	-20.18	-20.49
NGC 7460	14.10	1.39	13.69	3482	3.542	-20.12	-20.53
2342+06	14.70	1.03	14.41	5507	3.741	-20.51	-20.80
NGC 7750	13.70	1.64	13.23	3053	3.485	-20.23	-20.70
NGC 7756	13.80	1.14	13.47	3270	3.515	-20.28	-20.61
2346+05	15.30	1.50	14.86	3996	3.602	-19.22	-19.66
2348+00	14.30	2.93	13.61	8371	3.923	-21.82	-22.51
NGC 7780	14.70	1.75	14.21	5307	3.725	-20.43	-20.92
NGC 7782	13.10	1.50	12.66	5519	3.742	-22.12	-22.56
IC 1515	14.70	1.19	14.35	6856	3.836	-20.99	-21.34
IC 1516	14.20	1.00	13.92	7507	3.875	-21.68	-21.96

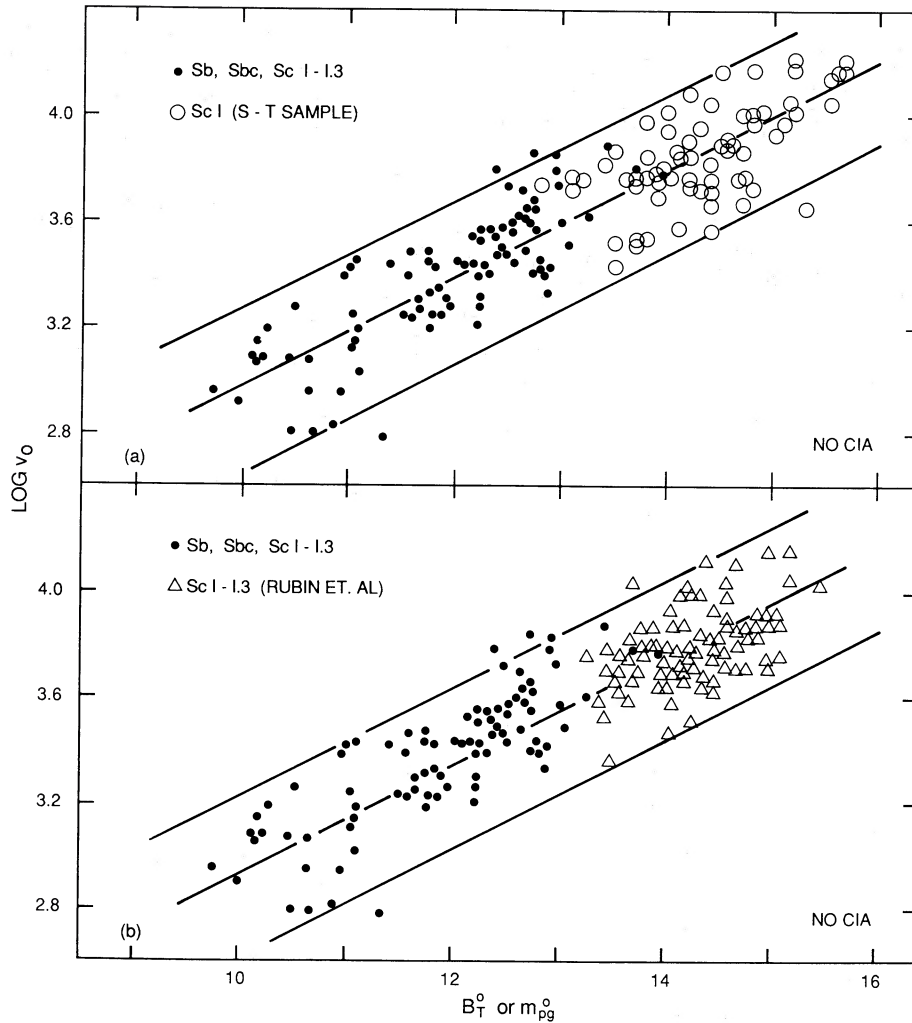


FIG. 5.—The Hubble diagram for Sb and Sc galaxies of the brightest luminosity class in the RSA (*closed circles*) combined with the two fainter catalogs of ScI galaxies. The faint S-T sample (*open circles*) is in the top panel. The faint Rubin *et al.* sample (*triangles*) is in the bottom panel. The ridge and envelope lines are drawn with a slope of 5.

V. THE ABSOLUTE MAGNITUDE DISPERSION FOR SCI GALAXIES FROM A NEAR VOLUME-LIMITED SAMPLE

If the data in Tables 1 and 2 were, indeed, to form a complete volume-limited sample, the standard deviation of the luminosity function could be found from the scatter in $B_T^{0,i}$ at a given v_0 in Figure 6. The least-squares regression lines there give $\sigma(B_T^{0,i}) = 0.53$ mag for the bright RSA sample alone about the mean relation $B_T^{0,i} = 3.186 \log v_0 + 0.657$, and $\sigma(B_T^{0,i}) = 0.56$ mag for the S-T faint sample alone about the equation $B_T^{0,i} = 2.338 \log v_0 + 4.995$. The standard deviation for the combined sample is $\sigma(M_{B_T^0}^{0,i}) = 0.70$ mag about the line $B_T^{0,i} = 4.445 \log v_0 - 3.38$. The slope of this last regression is not yet 5.0, showing that the sample is not entirely volume-limited, but this is not surprising because the data consist of two merged catalogs, each of which are only semicomplete themselves to particular flux levels (see footnote 6). *Imposing* a slope of 5 on the data in Figure 6 gives the ridge line that is drawn whose equation is $B_T^{0,i} = 5 \log v_0 - 5.30$. The magnitude residuals from this line give a standard deviation of

$$\sigma(M_{B_T^0}^{0,i}) = 0.72 \text{ mag}.$$

Another way to estimate the magnitude dispersion is to assume a particular form for $\Phi(M)$ and to calculate from it the predicted envelope lines in the bias diagrams of Figures 4 and 7 using the condition that $\Phi(M) = 1$ in each redshift interval. Because the volume increases as $v^2 \Delta v$, the normalization factor of $\Phi(M)$ becomes larger in each such interval by this volume factor, making the upper and lower envelope absolute magnitudes become brighter and fainter. If the form of $\Phi(M)$ is symmetrical about $\langle M \rangle$, these envelope lines will be mirror images about the $\langle M \rangle = \text{constant}$ mean line.

That this is approximately so is shown in Figure 10 which is similar to Figures 4b and 7b but with the envelope lines drawn to encompass most of the points, neglecting the four nearby galaxies near $\log v_0 = 2.8$. Figure 10 differs from Figure 4 in this neglect and also in using B_T^0 values uncorrected for internal absorption rather than $B_T^{0,i}$ as in Figure 4. A more appropriate lower envelope line in Figure 10, taking the fainter galaxies into account, would be drawn ~ 0.7 mag below that shown, giving the apex of the upper and lower envelopes to be between values $M_{B_T^0}$ of -20.8 and -20.4 , as used in § VI.

The envelope lines in Figures 4 and 10 have been drawn by

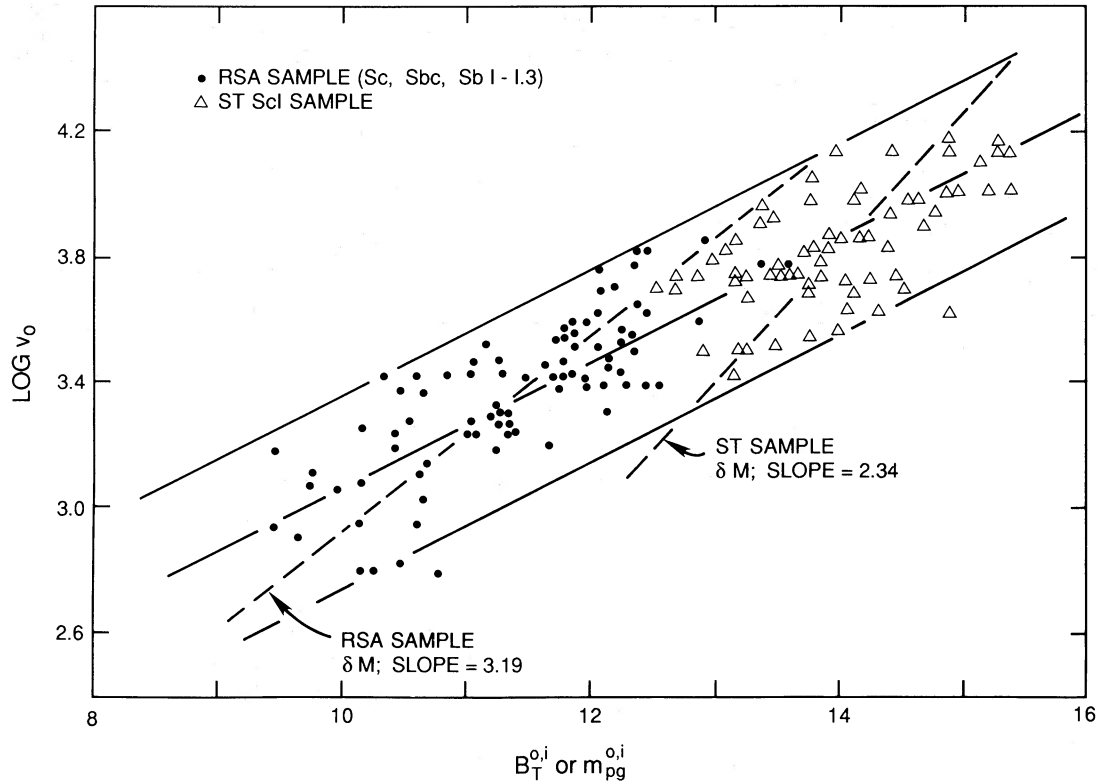


FIG. 6.—The Hubble diagram using fully corrected $B_T^{0,i}$ magnitudes and velocities, uncorrected for Virgo infall. Separate least-squares regressions for each sample, taking the residuals in magnitude rather than velocity give a slope to the RSA regression of 3.19 and a slope to the S-T sample of 2.34 respectively. The least-squares regression for the total data is $M_{B_T^{0,i}} = 4.445 \log v_0 - 3.38$ with a standard deviation of $\sigma(M) = 0.70$ mag. The ridge and envelope lines drawn have a slope of 5.0. The magnitude residuals about the ridge line of $B_T^{0,i} = 5.0 \log v_0 - 5.30$ have a standard deviation of $\sigma(M) = 0.72$ mag.

eye, and it is of interest to see how closely they agree with the expectation of the envelope shapes using an adopted form for $\Phi(M)$. Figure 11 shows the calculated envelope lines as if $\Phi(M)$ is a Gaussian with the $\sigma(M)$ dispersion values shown along the upper curves. To calculate the upper and lower M values that correspond to the $\Phi(M) = 1$ condition in each redshift interval requires an absolute volume normalization factor for $\Phi(M)$. For Figure 11 we have assumed that there are 1000 galaxies in the redshift interval of $\Delta \log v_0 = 0.2$ centered at $\log v_0 = 3.9$. It can be shown that for any other normalization we generate a second set of envelope curves that are identical with those in Figure 11 but with a constant difference in the $\log v_0$ abscissa. The curves in Figure 11 are, then, universal in the sense that they are *zero-point* free. They can be shifted both in ordinate and abscissa so as to envelope any particular data set in the M , $\log v_0$ plane such as that in Figures 4, 7, or 10. Of course, the independence of the envelope lines to the zero points of the ordinate or abscissa does not apply to the magnitude limit lines shown at $m = 13$ and 15.5 in Figure 11 relative to the envelopes. Obviously, these do depend on the M and the $\log v_0$ scale values, calculated from $m - M = 5 \log v_0 + 16.50$ (corresponding to $H_0 = 50$) to obtain their positions in Figures 4, 7, and 10.

The general shape of the calculated envelope lines in Figure 11 agrees well with the lines drawn by eye in Figure 10 showing that the assumption of a symmetrical Gaussian shape to $\Phi(M)$ is reasonable. A fit of Figure 11 curves to the Figure 7b data is shown in Figure 12 where we have shifted the envelope family of Figure 11 both in abscissa and ordinate for a best fit to the data by eye.

Although the data points do not fill the enclosed area partic-

ularly well at the faint end in Figure 12, it is here that the data in Tables 1 and 2 are expected to be most incomplete (cf. footnote 6 again). Clearly it will be of the greatest interest to apply the test in Figure 12 to the complete all-sky redshift surveys now in progress that reach a fixed flux level as faint as say $m = 15$. Figure 12 shows that if $\sigma = 0.7$ mag, then a volume-limited sample of Scl type galaxies should appear as a subset of a sample that is flux-limited at $m = 15$ out to redshifts of $\log v_0 \sim 3.5$ (or $v_0 = 3200 \text{ km s}^{-1}$). A study of the distribution of M_i in such a sample using this redshift restriction will give $\Phi(M)$ directly, which is surely a next step in this problem.

The fit of the calculated curves to the data in Figure 12 shows that $\sigma(M) \sim 0.6$ to 0.7 mag is a good fit, provided that $M_{B_T^{0,i}}(H_0 = 50) = -21.4$ is used for the apex to the envelopes (i.e., in the $v \rightarrow 0$ limit). This value of σ agrees with $\sigma(M) = 0.72$ mag from the direct calculation using magnitude residuals in Figure 6. It is this large σ value which leads to the large Malmquist bias implied in Figure 4a, the apparent increase of h_i with redshift in the top panels of Figures 8 and 9, the apparent multivalued h_i values at a given redshift in the bottom two panels of Figure 8 using method (2), and the broadness of the h_i distribution at a given redshift in the bottom panels of Figure 9 in the approximate volume-limited sample to $\sim 4000 \text{ km s}^{-1}$. This broadness in the h_i distribution is a direct consequence of the large $\sigma(M)$ of $\Phi(M)$.

VI. THE VALUE OF H_0 USING THE LOCAL CALIBRATORS

a) Photometric Data for the Three Calibrating Galaxies

The adopted photometric data for M31, M81, and M101 are listed in Table 3. Column (3) is the B_T magnitude as listed in

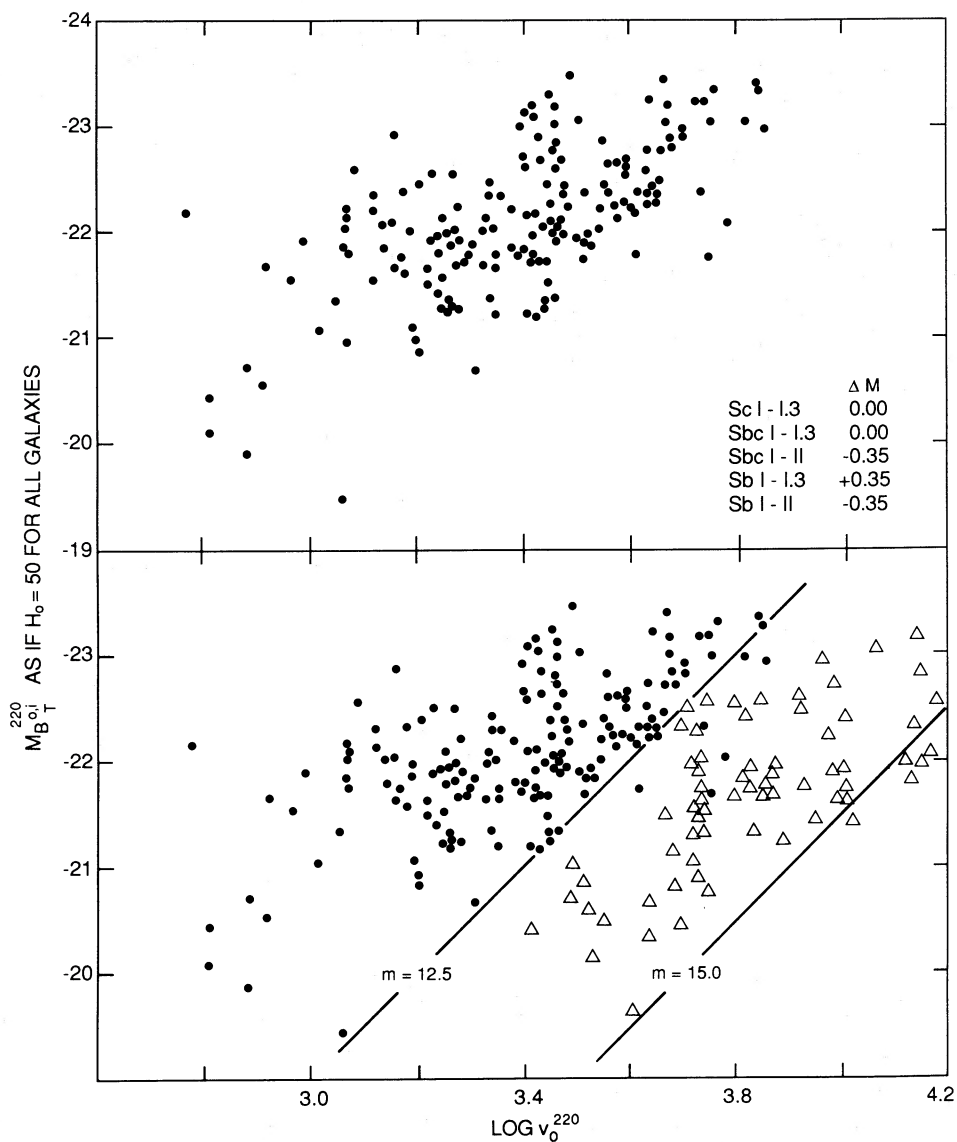


FIG. 7.—The Spaeenhauer bias diagram of M , $\log v$, similar to Fig. 1b, for the samples listed in Tables 1 and 2. *Top*: The RSA sample of Sb and Sc galaxies of bright luminosity classes with the data treated using method (1) of the text, reduced to the ScI-1.3 magnitude system. *Bottom*: The data of the top panel with the ScI data from the S-T sample of Table 2 added. The flux limit lines of $m = 12.5$ and 15.0 are shown. Similar to Fig. 4 but with the faint sample added. The apparent increase of $\langle M \rangle$ with increasing distance has now disappeared for the *total* sample.

TABLE 3
DATA FOR THE THREE CALIBRATING GALAXIES

Galaxy (1)	Type (2)	B_T (3)	A^0 (4)	B_T^0 (5)	A^i (6)	$B_T^{0,i}$ (7)	$(m-M)_{AB}^0$ (8)	M_{BT}^0 (9)	$M_{BT}^{0,i}$ (10)	$M_{B^0}^{ScI}$ (11)	$M_{B^0,i}^{ScI}$ (12)
M31	SbI-II	4.38	0.64	3.74	1.03	2.71	24.24	-20.50	-21.53	-20.85	-21.88
M81	SbI-II	7.86	0.07	7.79	0.78	7.01	28.7	-20.91	-21.69	-21.26	-22.04
M101	ScI	8.18	0.00	8.18	0.29	7.89	29.2	-21.02	-21.31	-21.02	-21.31
							Means	-20.81	-21.51	-21.04	-21.74

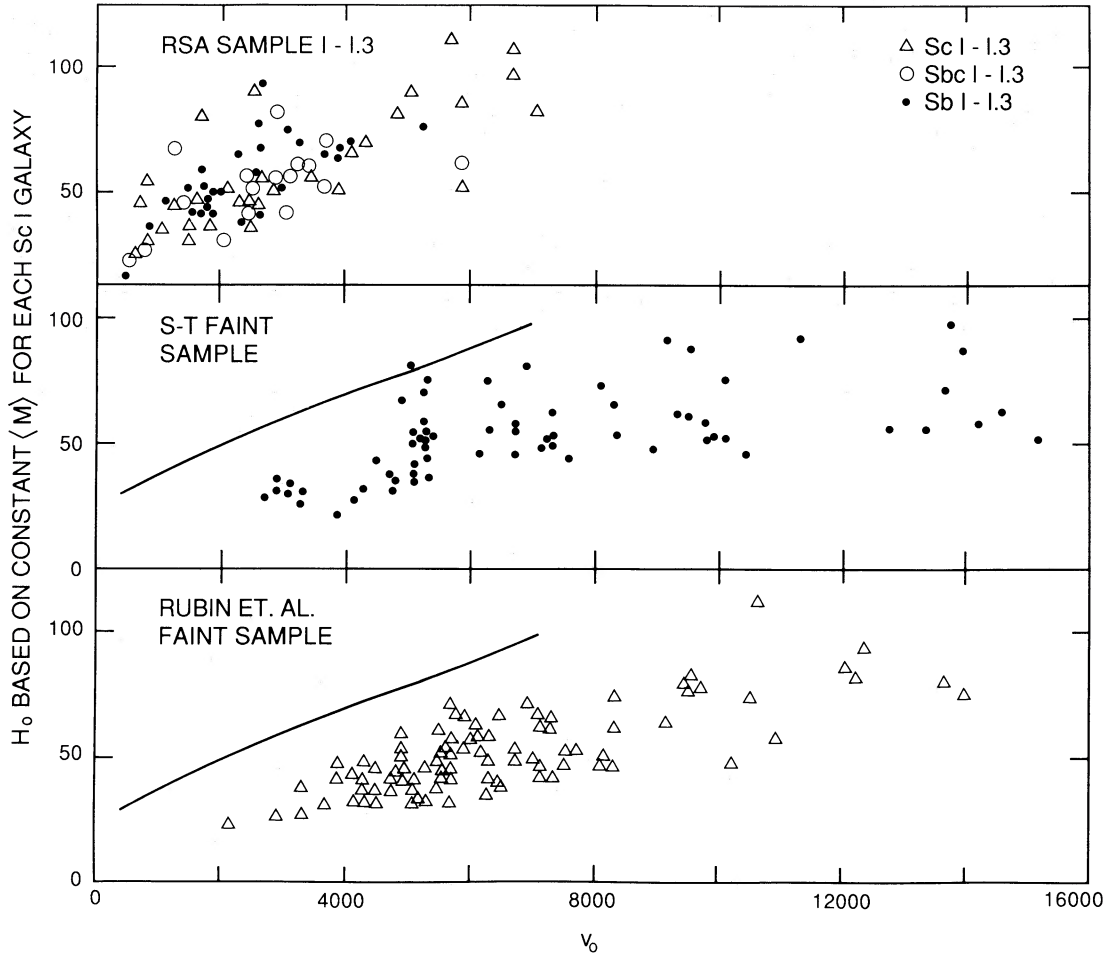


FIG. 8.—The apparent Hubble ratio v_0/r_1 , calculated by method (2) of the text in which a fixed $\langle M \rangle$ value is assigned to each galaxy in the sample. *Top*: The data for Sb, Sbc, and Sc galaxies from the bright flux-limited catalog of the RSA. *Middle*: Same as the top but for the faint ScI sample from S-T. The mean relation from the top panel is shown as the solid line. *Bottom*: Same as the middle panel but using the faint ScI sample from Rubin *et al.* (1976). The multivalued Hubble constant at a given distance for the combined sample is an artifact of the analysis that assigns $\langle M \rangle$ to each galaxy.

the RSA. The original source for these values is either Holmberg (1958) or de Vaucouleurs (1958), based on photographic integrations over the area covered by these large galaxies. Column (4) is the adopted correction for galactic absorption⁷ from column (13) of the RSA. Column (5) is column (3) corrected by column (4). The adopted mean correction to B_T^0 for internal absorption is in column (6), taken from column (14) of the RSA using the precept given on page 8 of that catalog.

The adopted apparent blue distance moduli, *corrected for galactic absorption alone*, are given in column (8), based on

⁷ The listed value of $A^0 = 0.64$ mag for M31 in the RSA requires special comment. This is obtained from the observed color excess of $E(B-V) = 0.16$ in the Baade-Swope (1963) field IV of M31, giving $A_B^0 = 4E(B-V) = 0.64$. The value differs from the cosec equation on p. 8 of the RSA that has been adopted for all other galaxies in the catalog. This equation would have given $A^0 = 0.21$ mag for M31. However, the reddening in M31 field is well determined from the Swope photometry that was calibrated photoelectrically. We adopt $E(B-V) = 0.16$ to be the total reddening due to galactic absorption alone. This is because field IV is far removed into the outskirts of M31, resembling fields in IC 1613, SMC, LMC, Sextans A, etc., where the internal reddening is known to be negligible over the face of most of these galaxies. The statement that the listed value of A^0 for M31 in the RSA “appears to be a misprint” (de Vaucouleurs and Corwin, 1986b, footnote 2) is, then, not the explanation of this entry for M31.

Cepheid variables as taken from a review by Tammann (1987). Combining columns (5) and (8) gives column (9) for $M_{B_T}^0$. Applying a correction of 0.35 mag to convert the Sbl-II absolute magnitude system to that of ScI galaxies (discussed in § II and shown in the code to Figs. 2 and 7, based on data in Table 1) gives the $M_{B_T^0}^{\text{ScI}}$ values listed in column (11).

The galaxian absolute magnitudes corrected for the internal absorption A^i are listed in column (10), found by subtracting column (6) from column (9), a procedure requiring a comment. The A^i values are those which are expected to apply to an average taken over the entire galaxy face so as to reduce B_T to what would be observed, B_T^i , in the absence of all internal absorption. The A^i value must not be applied to $(m - M)_{AB}^0$ to obtain the true modulus because Cepheids or brightest stars do not suffer the total A^i values. For example, $A^i \approx 0$ in the Baade-Swope field IV of M31, hence their $(m - M)$ value (corrected for galactic absorption alone) is the true modulus for Andromeda. The Cepheids and the brightest stars that have been observed in M81 and M101 are the brightest found and, in the absence of additional information we make the same assumption as for M31 that the $(m - M)_{AB}^0$ value in column (8) must not be corrected by the A^i value (col. [6]) that applies in correcting the B_T value to B_T^i . Justification to take the $(m - M)$ value in column (8) as the presently best value for the true

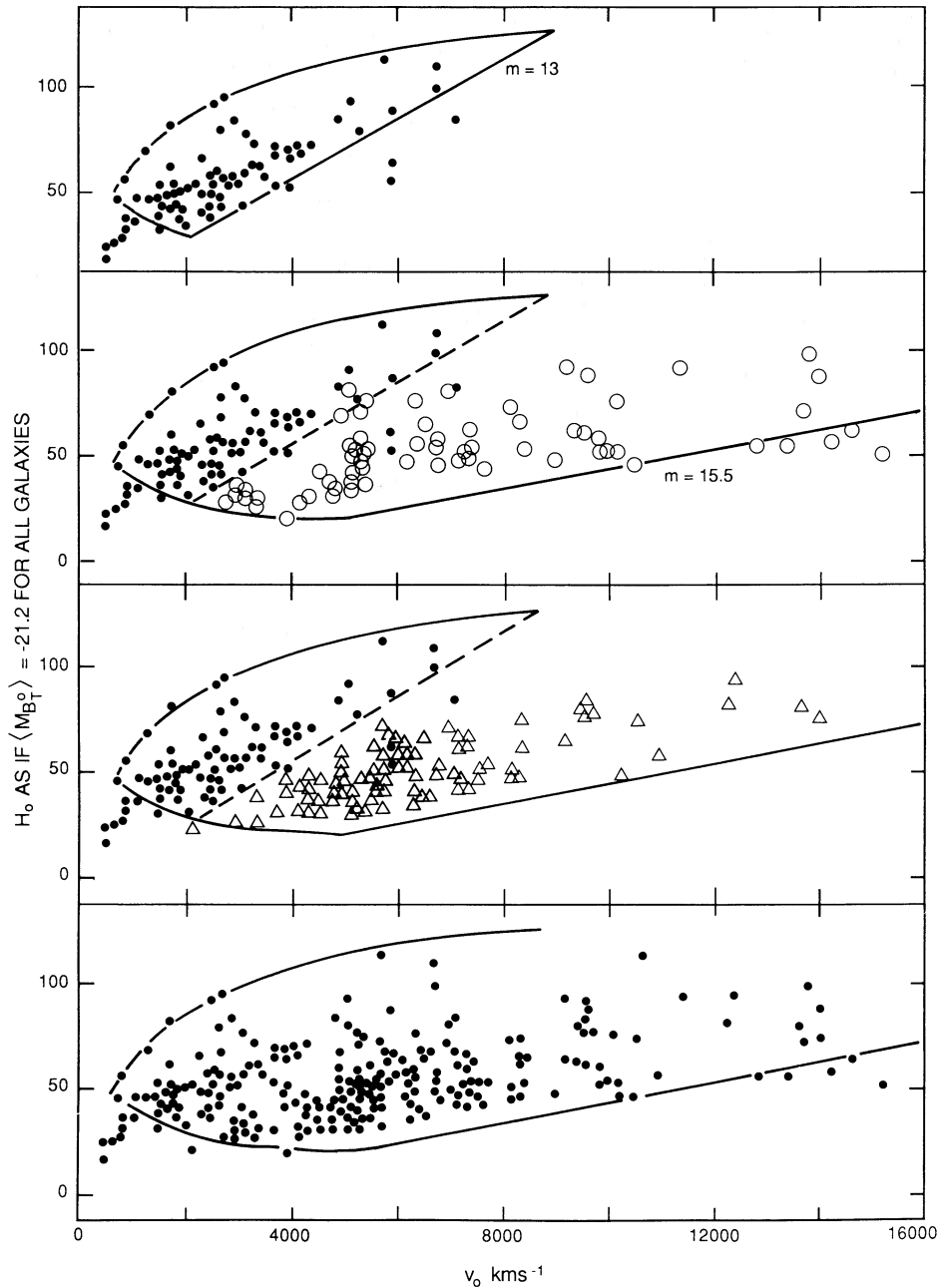


FIG. 9.—*Top*: Same as Fig. 8 for the RSA sample alone but now with an upper envelope line and the line for a flux limit of $m = 13.0$ drawn. (*b*) Same as top panel but with the S-T sample of Table 2 added, calculated by method (2) which assigns a fixed $\langle M \rangle$ value to every galaxy. The $m = 15.5$ flux limit line is shown. (*c*) Same as panel (*b*) but using the Rubin *et al.* ScI sample from data listed in their catalog. *Bottom*: The RSA sample of the top panel to which the S-T and the Rubin *et al.* ScI samples have been added. The $m = 15.5$ flux limit line is drawn. Note that the data approach a distance-limited sample for $v_0 \lesssim 5000 \text{ km s}^{-1}$, from which a bias-free value of H_0 near $50 \text{ km s}^{-1} \text{ Mpc}^{-1}$ can be deduced if $\langle M_{\text{ScI}} \rangle = -21.2$.

modulus that can be defended on principle is not only based on the M31 case (data from field IV), but also from NGC 2403. The Cepheid *apparent modulus* of $(m - M)_{\text{AB}} = 27.6$ for NGC 2403 (Tammann and Sandage 1968) has been found to be close to the true modulus (McAlary and Madore 1984) (actually is somewhat *smaller*) rather than to be only the apparent blue modulus as initially claimed by Madore (1976).

The magnitudes in column (12) of Table 3 for M31 and M81 are those listed in column (10) but again corrected by 0.35 mag brighter to put them on the ScI system.

b) Table 3 Values Applied to the Table 1 and 2 data

The most transparent way to use the calibrations of Table 3 to find H_0 would be to apply the column (9) or (11) values to the ridge lines of Figures 5a and 5b (no CIA), and/or columns (10) or (12) to the ridgeline of Figure 6 (has CIA) as if there was no bias effect (cf. Sandage and Tammann 1984, 1985, 1986). The equation of the ridge line in Figure 5a is $B_T^0 = 5 \log v_0 - 4.85$ which, with $\langle M_{B_T}^0 \rangle = -20.81$ from Table 3 (col. [9]) gives $H_0 = 64 \text{ km s}^{-1} \text{ Mpc}^{-1}$. Using the reduced value in

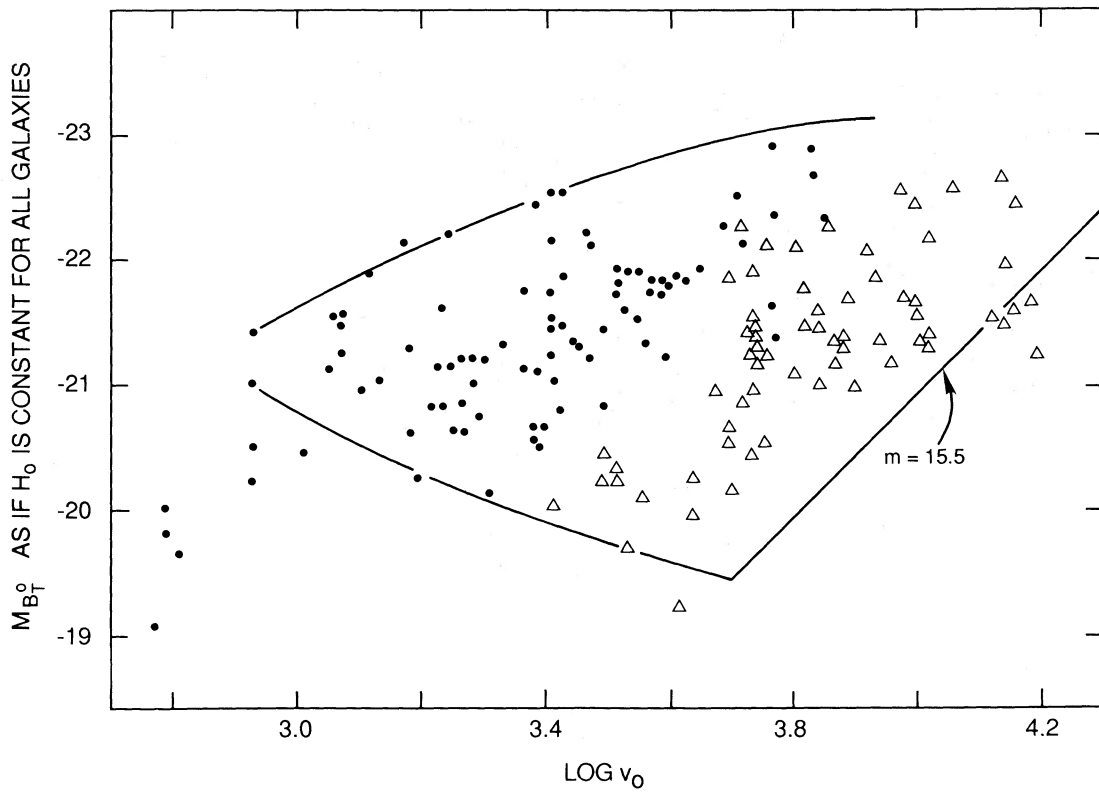


FIG. 10.—The M , $\log v_0$ bias diagram for the RSA sample (closed circles) and the S-T fainter ScI sample (Triangles). Envelope lines are shown, put by eye. The flux limit line is put at $m_B = 15.5$. A more realistic lower envelope line that encompasses the faintest seven galaxies with $\log v_0 \leq 3.1$ gives $M_{B_r}^0$ (apex) between -20.8 and -20.4 , used in Table 4.

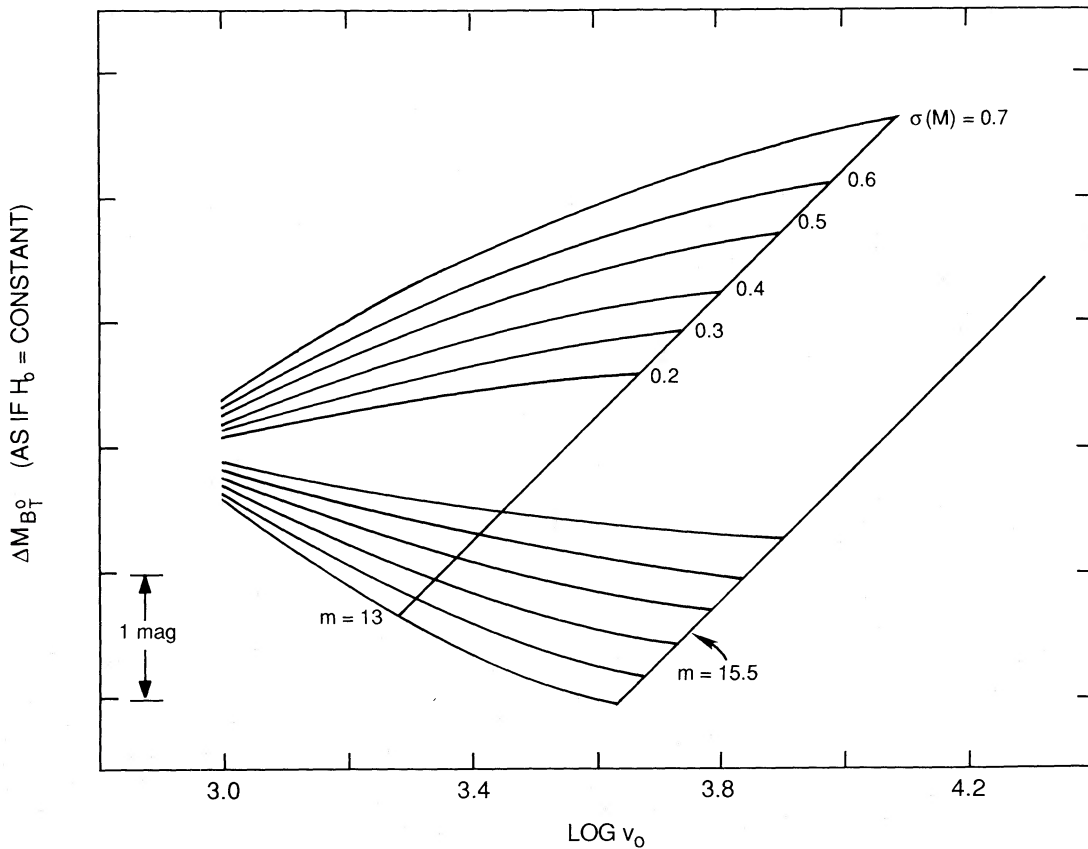


FIG. 11.—Theoretical envelope lines in the M , $\log v_0$ bias diagram calculated using symmetrical Gaussian $\Phi(M)$ luminosity functions with marked $\sigma(M)$ values.

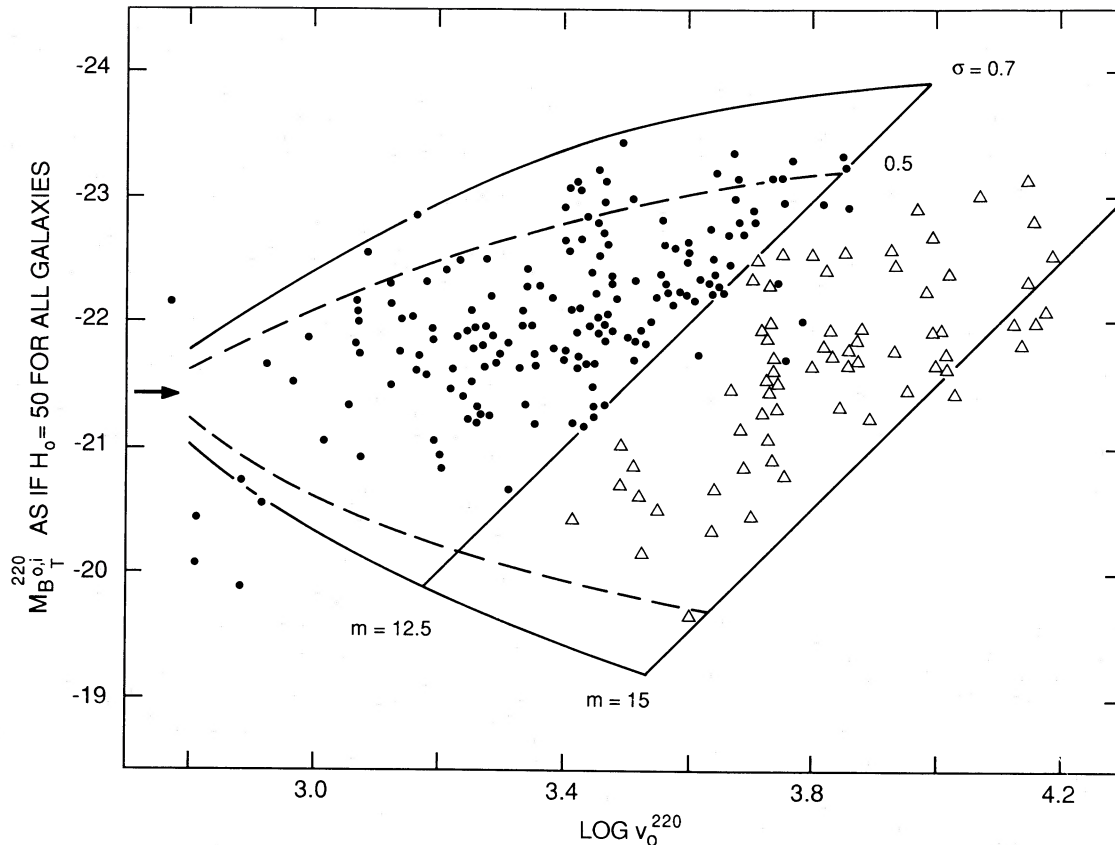


FIG. 12.—Superposition of Fig. 11 on the data of Fig. 4b, showing an apex absolute magnitude of $\langle M_{B_T}^{220} \rangle = -21.4$ used for the calculations in Table 4. Circles: data from the RSA (Table 1 here); triangles: data from the faint S-T ScI sample (Table 2).

column (11) of -21.04 gives $H_0 = 58 \text{ km s}^{-1} \text{ Mpc}^{-1}$, again neglecting the bias. Using the data corrected for internal absorption with the ridge line of Figure 6 whose equation is $B_T^{220} = 5 \log v_0 - 5.35$, and the calibrations of $\langle M_{B_T}^{220} \rangle = -21.51$ and $\langle M_{B_T}^{220}(\text{ScI}) \rangle = -21.74$ from columns (10) and (12), give $H_0 = 59$ and $H_0 = 53$, respectively.

However, the Malmquist bias is present even in the ridge lines of Figures 5 and 6b (see Sandage and Tammann [1974] for a similar discussion with an independent calibration of $M_{B_T}^{220}$ and a different correction procedure for the bias, that gave $H_0 = 57$). Merely applying the mean magnitudes from Table 3 to these ridge lines gives only an upper limit to H_0 .

With only three calibrators we have no way of knowing where within the scatter of the luminosity function the mean values in Table 3 lie. Because all three galaxies are nearby, they define an average for a sample as the volume approaches zero. Hence, the Table 3 values must be applied to the data in Figures (4), (10), and (12) at the apex of the envelope lines, i.e., in the $v_0 \rightarrow 0$ limit. This apex point is not well defined by our present data set because the envelope lines can be drawn in several ways that give a range for the apex position. Figures 4, 10, and 12 show different ways to encompass the points.⁸

In Figure 4 where the five faint galaxies near $\log v = 2.8$ are

⁸ Several commentators (Koo, Faber, Green) on an early draft of this paper suggested that the apex magnitude could be obtained from the data in Figures 10 and 12 by analysis of the distribution of M_{B_T} in given redshift intervals. Because our catalogs are incomplete (footnote 6) the apparent distribution function $f(M, v_0)$ from these data are poor representations of the true function, which can only be found from a complete survey of ScI galaxies to faint magnitudes, a feasible project but one not yet accomplished.

considered, the apex point is at $M_{B_T}^{220} = -21.0$ (if $H_0 = 50$). In Figure 12 where the three faintest galaxies are ignored, the apex point is drawn at $M_{B_T}^{220} = -21.4$ (again if $H_0 = 50$). Because both these values are fainter than the mean values in columns (10) and (12) of Table 3, the true value of H_0 must be smaller than our arbitrarily assumed value of 50. The range of H_0 from these apex values and from the calibration of -21.51 and -21.74 for $\langle M \rangle$ from Table 3 is listed in Table 4. The mean value from this section of Table 4 is $H_0 = 41.3$ as if all entries using $\langle M_{B_T}^{220} \rangle$ are equally probable.

Results of the same procedure applied to the data in Figure 10, uncorrected for internal absorption (Figs. 3 and 5), using the different lower envelopes mentioned in the last section, are listed in the second part of Table 4 using the two calibrations of Table 3, columns (9) and (11).

There is no formal way via statistics to put a rigorous error budget on the final mean value of $H_0 = 42 \text{ km s}^{-1} \text{ Mpc}^{-1}$. There are, however, reasonable limits on the uncertainties in (1) the Table 3 calibration of $\langle M \rangle$, and (2) the apex value of M as if $H_0 = 50$ in Figures 4, 10, and 12.

The outside limits of these errors are taken to be $\sim \pm 0.4 \text{ mag}$ for each, suggesting a total error of $\sim \pm 0.6 \text{ mag}$.⁹

⁹ To determine the range of error of the envelope fits to Figures 10 and 12, the referee ran Monte Carlo simulations of the $M, \log v$ diagram using a Gaussian $\phi(M)$ with $\sigma = 0.65 \text{ mag}$. From seven such simulations, which were sent with the referee's report, eye fits of the envelope lines, taken from Figure 11, were made with an initial blind eye to the ordinate. The range of the apex magnitude found in these seven fits was less than 0.2 mag, suggesting that the envelope fits we have made in Figures 10 and 12 do, in fact constrain the apex M_B value to better than the guessed value of 0.4 mag. I am grateful to the referee for this determination of the envelope fitting error.

TABLE 4
VALUES OF H_0 USING M_{Br} AT THE APEX OF THE SPAENHAUER DIAGRAM

Apex M_{Br}^o As if $H_0 = 50$	Source	Adopted M_{Br}^o Calibration	Required H_0	Apex M_{Br}^o As if $H_0 = 50$	Source	Adopted M_{Br}^o Calibration	Required H_0
-21.0.....	Fig. 4	-21.51	39.5	-20.4	Figs	-20.81	41.4
-21.0.....	Fig. 4	-21.74	35.6	-20.4	10+11	-21.04	37.2
-21.4.....	Fig. 12	-21.51	47.5	-20.8	Figs	-20.81	49.8
-21.4.....	Fig. 12	-21.74	42.7	-20.8	10+11	-21.04	44.8
		Mean	41.3			Mean	43.3

If $\langle H_0 \rangle = 42 \text{ km s}^{-1} \text{ Mpc}^{-1}$ is the best mean value from Table 4, then the 0.6 mag uncertainty corresponds to a factor of ± 1.3 times this value for the error in H_0 giving a final result as

$$H_0 = 42 \pm \sim 11 \text{ km s}^{-1} \text{ Mpc}^{-1}.$$

This corresponds to an inverse Hubble constant of

$$H_0^{-1} = (23.2 \pm 6) \times 10^9 \text{ yr} \quad (1)$$

for the Hubble time.

VII. THE VALUE OF Ω_0 FROM THE TIME SCALE TEST

a) Age of the Galactic Globular Clusters

Catalogs of isochrones for main-sequence turn-off ages using different Y and Z values include those of Simoda and Iben (1970), Iben and Rood (1970), Ciardullo and Demarque (1977), Vandenberg (1983), and Vandenberg and Bell (1985). Cluster ages using these isochrones require absolute calibration of cluster distances so as to change apparent magnitudes to absolute luminosities.

Most of the differences between various reviews of cluster ages (cf. Demarque 1979; Sandage 1982; Vandenberg 1986) at fixed chemical composition are due to different assignments of cluster distances, and hence to differences in L_{TO} , rather than to differences in the isochrones calculated by the different groups. An example are the ages discussed by Demarque (1979) that average ~ 13.5 Gyr compared with ~ 17 Gyr for the same clusters (Sandage 1982). This $\sim 25\%$ difference can be traced to distance moduli that differ by ~ 0.24 mag for the same clusters (Table 1 of Demarque [1979] compared with Table 2 of Sandage [1982]).

The mean age of ~ 17 Gyr from the Yale (or Vandenberg) isochrones are based on distance moduli that used $M_V = 0.63$ for RR Lyrae stars of Oosterhoff group II, and 0.80 mag for those of group I (Sandage 1982, Table 2 and § VIIIb). The most recent statistical parallax values of $M_V = 0.76 \pm 0.14$ (Hawley *et al.* 1986) or $M_V = 0.86 \pm 0.14$ (Barnes and Hawley 1986) for field RR Lyraes, averaged over the Oosterhoff types, believe values 0.2 mag brighter than this RR Lyrae calibration that gives $T_c = 17$ Gyr. However, it now seems likely that the globular cluster ages are, in fact, ~ 14 Gyr, rather than 17 Gyr, based on new data on the chemical abundances of low-metallicity stars, rather than on a change in $M_V(\text{RR})$.

Simoda and Iben (1968) were the first to show that varying the CNO abundance at fixed Z abundance has the same effect on the ages as varying the average Z value. This is because a significant fraction of the opacity comes from the CNO elements. This means that for a fixed main-sequence turn-off luminosity, L_{TO} , an increased CNO abundance means decreased age, keeping Y and the remaining heavy elements, Z , constant. Hence, the age depends on L_{TO} , Y , Z , and the $[O/Fe]$ ratio.

Explicit calculations of the effect of varying $[O/Fe]$ at fixed Y , and Z have been made by Rood (1978), by Rood and Crocker (1985), by Vandenberg and Demarque (quoted in Demarque 1979), and by Vandenberg (1985, 1986). In the last references Vandenberg concludes that the age at a given L_{TO} is decreased by 15% as $[O/Fe]$ changes from 0.0 to 0.5.

Observational evidence has become convincing that $[O/Fe]$ progressively increases from 0.0 to ~ 0.5 as $[Fe/H]$ decreases from 0 to -1 ; thereafter $[O/Fe]$ may remain at about $+0.5$ as $[Fe/H]$ decreases further. Part of the evidence is from Lambert, Sneden, and Ries (1974), Sneden, Lambert, and Whitaker (1979), Clegg, Lambert, and Tomkin (1981), Leep and Wallerstein (1981), Barbury (1983) and others. Reviews are given by Sneden (1985), Barbury (1985), Kraft (1985), and Matteucci (1986). The reason for the increased $[O/Fe]$ abundance ratio in low $[Fe/H]$ stars appears to be enhanced oxygen production in explosive nucleosynthesis (Arnett 1978) in massive stars. The abundance ratios $[M/Fe]$ early in the Galaxy differs from the ratios in the later chemical input produced by an IMF that is now peaked toward later ejecta from lower mass stars (cf. Twarog and Wheeler 1982).

With $[O/Fe]$ adopted to be $+0.5$ for globular cluster stars, assuming the oxygen effect to be the same as in field subdwarfs, and using the estimates of the effect given by Vandenberg of a $\sim 15\%$ age reduction, the earlier estimates of ~ 17 Gyr are reduced to 14.5 Gyr.

However, a more secure value comes from the high weight age measurement of 47 Tuc where the values of Y , $[Fe/H]$, $[O/Fe]$, and the distance are optimized to fit the predicted $C-M$ diagram over its entire range (Hesser *et al.* 1987). These authors estimate the age of 47 Tuc to be 13.5 ± 1 Gyr, which is probably the most accurate age determination made to date. For all the standard reasons (Sandage 1982) we adopt this to be the age of the globular system in the Galaxy, to which we must now add the gestation time of galaxies to find the age of the universe.

b) The Cosmological Time Scale Test

The gestation time of globular clusters, counted from the creation event, must be added to the globular cluster ages to obtain the age of the universe. One way to estimate this is to determine the look-back time to the highest redshift gravitational potential wells that eventually have become galaxies.

Quasars are known to redshifts of 4.0. Because quasars are events in the nuclei of galaxies, galaxian potential wells must have existed at least this look-back time ago. Objects at a redshift of 4 have a look-back time of between 0.80 and 0.91 of the age of the universe, T_U , depending on the value of Ω between 0 and 1 (Sandage 1961b, Table 2). Therefore, the gestation time of galaxies is no longer than either 20% (for $\Omega_0 = 0$) or 9% (if $\Omega_0 = 1$) of T_U .

Later in this section we obtain $\Omega_0 \approx 1$ by an iteration and $T_U \approx 15$ Gyr for the age of the universe, requiring thereby a galaxy gestation time that is shorter than $\sim(0.09)$ (15) ~ 1.4 Gyr. This, then, taken at its upper limit and added to the age of the globular cluster system of the Galaxy, gives the age of the universe to be

$$T_U = 14.9 \pm 2 \text{ Gyr}, \quad (2)$$

where we have adopted the Hesser *et al.* uncertainty of 1 Gyr for 47 Tuc and have doubled it for the uncertainty of the galaxian gestation period.

Equation (1) for the Hubble time of $H_0^{-1} = (23.2 \pm 6)$ Gyr together with equation (2) gives then

$$H_0 T_U = 0.64 \pm 0.19 \quad (3)$$

where the listed error is the combination of the quoted 26% uncertainty in H_0 and the quoted 13% uncertainty in T_U .

The time ratio $H_0 T_U$ is a function only of Ω_0 if $\Lambda = 0$, where the values are listed elsewhere (Sandage 1961a, Table 8). Interpolation in this table for the "dust universe" with $H_0 T_U$ from equation (3) gives

$$\Omega_0 = 1.2_{-0.9}^{+3.0} \quad (4)$$

where we have taken the upper and lower limit on Ω_0 to be 0.81 and 0.47 using the 29% error¹⁰ given by equation (3).

¹⁰ Adopting a less pessimistic error budget to H_0 by assigning 0.3 mag rather than 0.6 mag to the uncertainties in $\langle M \rangle$ from both the calibrators and the apex magnitude, gives $H_0 = 42 \pm 6$. This smaller error of 14% together with the 13% error in T_U propagates to the time ratio as $H_0 T_U = 0.64 \pm 0.12$. This constrains Ω_0 more tightly to $\Omega_0 = 1.2_{-0.7}^{+1.6}$. To obtain Ω_0 more accurately than this via the time scale test will be more difficult than the work to date, because it seems unlikely that the true errors in H_0 and T_U can be pushed much below 10% to 15%, which still propagates to a large error in Ω_0 .

REFERENCES

- Aaronson, M., *et al.* 1982, *Ap. J. Suppl.*, **50**, 241.
 Arnett, D. W. 1978, *Ap. J.*, **219**, 1008.
 Baade, W., and Swope, H. H. 1963, *A.J.*, **68**, 435.
 Barbur, B. 1983, *Astr. Ap.*, **123**, 1.
 ———. 1985, in *Production and Distribution of C, N, O Elements* ed. I. J. Danziger, F. Matteucci, and K. Kjar (Garching: ESO), p. 49.
 Barnes, T. G., and Hawley, S. L. 1986, *Ap. J. (Letters)*, **307**, L9.
 Binggeli, B., Sandage, A., and Tammann, G. A. 1985, *A.J.*, **90**, 1681 (BST).
 Bothun, G. D., Aaronson, M., Schommer, B., Huchra, J., and Mould, J. 1984, *Ap. J.*, **278**, 475.
 Bottinelli, L., Gouguenheim, L., Paturel, G., and Teerikorpi, P. 1986, *Astr. Ap.*, **156**, 157.
 Brown, G. S., and Tinsley, B. M. 1974, *Ap. J.*, **194**, 555.
 Bruzual, A. G., and Spinrad, H. 1978, *Ap. J.*, **220**, 1.
 Ciardullo, R., and Demarque, P. 1977, *Trans. Yale Univ. Obs.*, Vol. **33**.
 Clegg, R. D., Lambert, D. L., and Tomkin, J. 1981, *Ap. J.*, **250**, 262.
 Demarque, P. 1979, in *IAU Symposium 85, Star Clusters*, ed. J. E. Hesser (Dordrecht: Reidel), p. 281.
 de Vaucouleurs, G. 1958, *Ap. J.*, **128**, 465.
 ———. 1972, in *IAU Symposium 44, External Galaxies and Quasistellar Objects*, ed. D. S. Evans (Dordrecht: Reidel), p. 353.
 de Vaucouleurs, G., and Bollinger, G. 1979, *Ap. J.*, **233**, 433.
 de Vaucouleurs, G., and Corwin, H. G. 1986a, *A.J.*, **92**, 722.
 ———. 1986b, *Ap. J.*, **308**, 487.
 de Vaucouleurs, G., de Vaucouleurs, A., and Corwin H. 1976, *Second Reference Catalog of Bright Galaxies* (Austin: University of Texas Press) (RC2).
 de Vaucouleurs, G., and Peters, W. L. 1986, *Ap. J.*, **303**, 19.
 Dressler, A., *et al.* 1987, *Ap. J. (Letters)*, **313**, L37.
 Giraud, E. 1985, *Astr. Ap.*, **153**, 125.
 ———. 1986a, *Ap. J.*, **301**, 7.
 ———. 1986b, *Ap. J.*, **309**, 512.
 Graham, J. A. 1976, *A.J.*, **81**, 681.
 Greenstein, J. L. 1938, *Ap. J.*, **88**, 605.
 Hawkins, G. S. 1962, *Nature*, **194**, 563.
 Hawley, S. L., Jeffreys, W. H., Barnes, T. G., and Wan, L. 1986, *Ap. J.*, **302**, 626.
 Hesser, J. E., Harris, W. E., VandenBerg, D. A., Allright, J. W. B., Shott, P., and Stetson, P. 1987, *Pub. A.S.P.*, **99**, 739.
 Hickson, P. 1977, *Ap. J.*, **217**, 964.
 Holmberg, E. 1958, *Medd Lund Obs.*, Ser. II, No. 136.
 Hubble, E. 1936a, *Ap. J.*, **84**, 158.
 ———. 1936b, *Ap. J.*, **84**, 270.
 ———. 1936c, *Ap. J.*, **84**, 517.
 Hubble, E., and Tolman, R. C. 1935, *Ap. J.*, **82**, 302.
 Humason, M. L., Mayall, N. U., and Sandage, A. 1956, *A.J.*, **61**, 97 (HMS).
 Iben, I., and Rood, R. T. 1970, *Ap. J.*, **159**, 605.
 Kapahi, V. K. 1975, *M.N.R.A.S.*, **172**, 513.
 ———. 1987, in *IAU Symposium 124, Observational Cosmology* ed. A. Hewitt, C. Burbidge, and L. Z. Fang (Dordrecht: Reidel), p. 251.
 Kennicutt, R. C. 1982, *Ap. J.*, **259**, 530.
 Kraan-Korteweg, R. C. 1986, *Astr. Ap. Suppl.*, **66**, 255.
 Kraan-Korteweg, R. C., Sandage, A., and Tammann, G. A. 1984, *Ap. J.*, **283**, 24 (KKST).
 Kraft, R. P. 1985, in *Production and Distribution of C, N, O Elements* ed. I. J. Danziger, F. Matteucci, and K. Kjar (Garching: ESO), p. 21.
 Lambert, D. L., Sneden, C., and Ries, L. M. 1974, *Ap. J.*, **188**, 97.
 Lasker, B. M. 1970, *A.J.*, **75**, 21.
 Leep, E. M., and Wallerstein, G. 1981, *M.N.R.A.S.*, **196**, 543.
 Loh, E. D., and Spillar, E. J. 1986, *Ap. J. (Letters)*, **307**, L1.
 Madore, B. F. 1976, *M.N.R.A.S.*, **177**, 157.
 Matteucci, F. 1986, *Pub. A.S.P.*, **98**, 973.
 Mattig, W. 1958, *Astr. Nach.*, **284**, 109.
 ———. 1959, *Astr. Nach.*, **285**, 1.
 McAlary, C. W., and Madore, B. F. 1984, *Ap. J.*, **282**, 101.
 Melnick, J., Terlevich, R., and Moles, M. 1987, preprint.
 Miley, G. K. 1971, *M.N.R.A.S.*, **152**, 477.
 Misner, C. W., Thorne, K. S., and Wheeler, J. A. 1973, *Gravitation* (San Francisco: Freeman) Exercise 29.6.
 Nicoll, J. F., and Segal, I. E. 1982, *Ap. J.*, **258**, 457.
 Oke, B. J., and Sandage, A. 1968, *Ap. J.*, **154**, 21.
 Refsdal, S., Stabell, R., and de Lang, F.-G. 1967, *Mem.R.A.S.*, **71**, 143.

- Robertson, H. P. 1955, *Pub. A.S.P.*, **67**, 83.
- Robertson, H. P., and Noonan, T. W. 1968, in *Relativity and Cosmology* (Philadelphia: Saunders), § 15.7.
- Rood, R. T. 1978, paper presented at the NATO Advanced Study Institute on Globular Clusters, Cambridge, England.
- Rood, R. T., and Crocker, D. A. 1985, in *Production and Distribution of C, N, O Elements* ed. I. J. Danziger, F. Matteucci, and K. Kjar (Garching: ESO), p. 61.
- Rubin, V. C., Ford, W. K., Thonnard, N., Roberts, M. S., and Graham, J. A. 1976, *A.J.*, **81**, 687.
- Sandage, A. 1961a, *Ap. J.*, **133**, 313.
- . 1961b, *Ap. J.*, **134**, 916.
- . 1962, *Ap. J.*, **136**, 319.
- . 1972a, *Ap. J.*, **173**, 485.
- . 1972b, *Ap. J.*, **178**, 1.
- . 1972c, *Ap. J.*, **178**, 25.
- . 1975, *Ap. J.*, **202**, 563.
- . 1982, *Ap. J.*, **252**, 553.
- . 1986, *Ap. J.*, **307**, 1.
- Sandage, A., Bingelli, B., and Tammann, G. A. 1985a, *A.J.*, **90**, 395 (STB).
- . 1985b, *A.J.*, **90**, 1759 (STB).
- Sandage, A., and Tammann, G. A. 1974, *Ap. J.*, **194**, 559.
- . 1975a, *Ap. J.*, **196**, 313.
- . 1975b, *Ap. J.*, **197**, 265.
- . 1981, *A Revised Shapley-Ames Catalog of Bright Galaxies* (Carnegie Inst. Washington Pub. 635).
- . 1984, in *Large-Scale Structure of the Universe, Cosmology, and Fundamental Physics, Proc. CERN Symposium*, (Geneva: CERN), p. 127.
- . 1985, in *Supernovae* ed. N. Bartel, (Lecture Notes in Physics No. 224), p. 1.
- . 1986, in *Inner Space—Outer Space, Proc. Fermilab Conference, May 1984*, (Chicago: University of Chicago Press), p. 41.
- . 1987, *A Revised Shapley-Ames Catalog* (2d ed.; No. 635).
- Sandage, A., Tammann, G. A., and Hardy, E. 1972, *Ap. J.*, **172**, 253.
- Sandage, A., Tammann, G. A., and Yahil, A. 1979, *Ap. J.*, **232**, 352 (STY).
- Segal, I. 1975, *Proc. Nat. Acad. Sci.*, **72**, 2473.
- . 1981, *Proc. Nat. Acad. Sci.*, **77**, 10.
- . 1982, *Ap. J.*, **252**, 37.
- Simoda, M., and Iben, I. 1968, *Ap. J.*, **152**, 509.
- . 1970, *Ap. J. Suppl.*, **22**, 81.
- Snedden, C. 1985, in *Production and Distribution of C, N, O Elements* ed. I. J. Danziger, F. Matteucci, and K. Kjar, (Garching: ESO), p. 1.
- Snedden, C., Lambert, D. L., and Whitaker, R. W. 1979, *Ap. J.*, **234**, 964.
- Solheim, J.-E. 1966, *M.N.R.A.S.*, **133**, 321.
- Soneira, R. M. 1979, *Ap. J. (Letters)*, **230**, L63.
- Spaenhauer, A. M. 1978, *Astr. Ap.*, **65**, 313.
- Stebbins, J., Whitford, A. E., and Johnson, H. L. 1950, *Ap. J.*, **112**, 469.
- Swarup, G. 1975, *M.N.R.A.S.*, **172**, 501.
- Tammann, G. A. 1987, in *IAU Symposium 124, Observational Cosmology* ed. A. Hewitt, C. Burbidge, and L. Z. Fang (Dordrecht: Reidel), p. 151.
- Tammann, G. A., and Sandage, A. 1968, *Ap. J.*, **151**, 825.
- Tammann, G. A., Yahil, A., and Sandage, A. 1979, *Ap. J.*, **234**, 775 (TYS).
- Teerikorpi, P. 1975a, *Astr. Ap.*, **45**, 117.
- . 1975b, *Observatory*, **95**, 105.
- . 1984, *Astr. Ap.*, **141**, 407.
- Twarog, B., and Wheeler, J. C. 1982, *Ap. J.*, **261**, 636.
- VandenBerg, D. A. 1983, *Ap. J. Suppl.*, **51**, 29.
- . 1985, in *Production and Distribution of C, N, O Elements*, ed. I. J. Danziger, F. Matteucci, and K. Kjar (Garching: ESO), p. 73.
- . 1986, in *IAU Symposium 136, Globular Clusters Systems Around Galaxies*, ed. J. Grindlay and A. G. D. Philip, (Dordrecht: Reidel).
- VandenBerg, D. A., and Bell, R. A. 1985, *Ap. J. Suppl.*, **58**, 561.
- van den Bergh, S. 1960a, *Ap. J.*, **131**, 215.
- . 1960b, *Ap. J.*, **131**, 558.
- Whitford, A. E. 1971, *Ap. J.*, **169**, 215.
- Zwicky, F. 1957, *Morphological Astronomy* (Berlin: Springer), pp. 220–228.
- Zwicky, F., and collaborators. 1961–1968, *Catalog of Galaxies and Clusters of Galaxies*, Vols. I–VII (Pasadena: California Institute of Technology).

ALLAN SANDAGE: Mount Wilson Observatories, Carnegie Institution of Washington, 813 Santa Barbara Street, Pasadena, CA 91101-1292